

Anonymous Referee #3 Received and published: 28 May 2015

This is a very interesting and original paper using the full spectrum reflectance (400- 900nm) to predict landscape-scale (or maybe it would be better “ecosystem-scale”?) CO₂ fluxes at a pasture and at a rice field. PLSR using reflectance values is without doubt providing high potential, as it is exploiting all the spectrum in the VIS-NIR, and this is clearly demonstrated in the paper. In particular, relevant information on the predictive power of spectral observations at increasing flux integration intervals are provided. However, the paper is not providing any type of comparison between the PLSR presented method and the “traditional” Spectral Vegetation Index (SVI) approach in estimating carbon fluxes. A simple graph/table comparing the performance of PLSR with a few standard indices which showed a good performance according to many authors such as e.g. Gitelson, Rossini, etc. (such as NDVI, NDVIgreen, NDVIred edge e.g. based on MODIS, Sentinel2 bands) would be of great interest to the reader. I understand that this is not the main focus of the study, but this additional information would, in my view, significantly strengthen the paper.

We agree with this point, and have added Table 3 (attached as a Figure to this comment), comparing the correlation of SVIs with the carbon flux measurements from this study. Using the same method of training with a random 80% of the dataset and validating with 20% of the dataset, we evaluated both the training correlation between GPP and NEE and the predictive power of the resulting relationships with SVIs. For SVIs, we tested NDVI (Rouse et al 1974), MODIS NDVI, NDVIgreen (Gitelson et al 1996), NDVIrededge (Gitelson & Merzlyack 1994), and PRI (Gamon 1992). For Table 3, we included the training and validation correlation (R²) for the MODIS NDVI because of its wide applicability and NDVIrededge because it had the highest training and validation R² values for the tested indices. The full range of statistics for all the SVIs will be included as a Supplementary Table.

Overall, the SVIs performed reasonably well at predicting CO₂ fluxes at all the sites and at the Rice, although R² values were lower than those obtained by PLSR modeling. At the Pasture, PLSR modeling significantly outperformed the predictive power of SVIs, due to the increased canopy complexity at this site. We now include a comparison of SVI performance versus PLSR performance in the Discussion section.

In similar studies estimating biophysical parameters, in fact, the PLS models performed equally - or slightly better- compared to the best indices based on e.g. exponential curve fitting. To this regard, it would be good to add a discussion on the advantages and disadvantages (expected -in the introduction- and observed -in the analyzed datasets discussion-) of using full spectrum PLSR vs. SVIs more traditional approaches. Despite being very promising, the PLSR method may not be able to “read” some important information contained in the spectrum. Optical sampling is based on reflectance information, but it is mostly focused on relative values rather than reflectance values themselves. Hence, it should be mentioned that to retrieve relevant information, the reflectance values in the SVI approach are generally weighted against a reference band, as in the case, for instance- of CIred-edge, PRI or WBI. This is one of the reasons why the “best” bands for PLSR may not correspond to the “best” bands for SVIs. Also, normalisation in the SVI approach is used and it is also important e.g. to limit the effects of slightly different illumination conditions during the different observation days when spectral

measurements are carried out: reflectance temporal trends can be a bit noisy, but normalised SVIs trends are generally much less affected by noise.

This point is well taken, and we have added a brief discussion at the end of Discussion 4.1 pointing to some of the differences and limitations of SVIs compared with PLSR methods. In particular we address this comment regarding the limitations of PLSR in comparison with SVIs when reflectance spectra are noisy.

Specific comments

Methods/Site Characteristics section 2.1, page 5085: adding some photos of the investigated sites/instrumentation would help the reader understanding the site and the measurements characteristics such as spatial heterogeneity, measurements set ups, etc.

We now point the reader to Figure 3 within this section, which includes four photographs of typical field conditions to understand site heterogeneity.

Section 2.2: a discussion regarding the bi-hemispherical reflectance measurements advantages and limitations and the possible impact in the authors' observations could be added (see e.g. Meroni et al, 2011 - REVIEW OF SCIENTIFIC INSTRUMENTS).

We agree with this comment, and have added a brief description of the use of bi-hemispherical reflectance filters in the Methods section 2.2. We point out that the use of bi-hemispherical reflectance filters limit the amount of soil reflectance at high solar angles compared to unfiltered reflectance measurements, but that bi-hemispherical filters can have a slight impact on reflectance measurements collected in early morning or evening.

At page 5092, the authors mention that intra-site variability during an individual sampling event is particularly high in the NIR. The authors should explain more in detail why this is happening.

We have added a sentence to this section indicating that the higher NIR variability at the pasture site is due to higher spatial variability in canopy structure at the pasture compared to the rice paddy, which is a monoculture with a simple crop phenological cycle.

Page 5093: "The NIR reflectance at the pasture had a stable mean during the year". This comment is quite general. It would be better to analyze and discuss the NIR trends and explain the variations more in detail. Maybe adding a trend of a simple greenness SVI -such as NDVI- would help to identify and clarify the complexity of the VIS-NIR wavelengths response to canopy phenology.

Page 5094: It is interesting to see that for shorter timescales is the highest VIP score at around 700nm, while for longer timescales NIR is providing more relevant information. According to such results, spectral regions related to structure (and not to chlorophyll absorption) provide relevant information to monitor GPP. This finding was also presented in a BG discussion paper by Balzarolo et al. (<http://www.biogeosciencesdiscuss.net/11/10323/2014/bgd-11-10323-2014.pdf>) and I think should be discussed by the authors.

Thank you for pointing us to this recent paper, and we now include it in our Discussion section.

Page 5096: to investigate temporal trends, measurements should be carried out at fixed points. This should be highlighted and discussed in more detail in the paper.

We believe that we have adequately described our sampling methods at each site within Methods section 2.2. Spectra were captured at randomized locations within the flux footprint during each sampling date in order to best match the spatial scale of the CO₂ flux measurements, which measure ecosystem processes at the landscape-scale.

Page 5099, line 5: is the Pasture (as it is not irrigated) water limited and sometimes affected by water stress? This maybe would explain part of the variability which is not explained by the model.

This is a good point, and we have added this possible explanation to our list of ecosystem processes that make predicting CO₂ flux with canopy reflectance at the Pasture more complex than the Rice.

Page 5101, line 26: "... could be used in conjunction with a spectrometer capable of making wider spectral reflectance measurements at eddy covariance sites to evaluate areas of the NIR spectrum at longer wavelengths". As in the previous lines you were mentioning the importance of investigating the "infrared area" correlated with structural components and fiber, lignin, cellulose. Did you mean SWIR instead of NIR? Within the EUROSPEC Cost Action, a spectrometer measuring in the SWIR was developed (Sensors 2015, 15(1), 1088-1105; doi:10.3390/s150101088)

Yes, we did mean the SWIR region, and now include this new paper as a reference within this section.

Reviewer #4:

General comments: The authors report on a study within which they quantified hyperspectral reflectance and CO₂ fluxes over five years at a pasture and a rice field in California. The main aims of the study are to assess the seasonal and interannual variability in hyperspectral reflectance and the associated links to GPP and NEE. To this end the authors use partial least squares regression modelling. The study relies on an impressive data basis; methods are standard and sound; results are clear and the discussion makes appropriate reference to the pertinent literature; the paper is well written, at times the style could be more concise however. Taken together this study represents a useful addition to the literature and I have only a few smaller comments, listed below.

Detailed comments:

p. 5080, l. 10: spectra are discrete, not continuous; the term "continuous" is used quite frequently throughout the paper – in my view almost no measurements are truly continuous but rather continuous in theory and in practise interrupted by unavoidable gaps; bottom line – I suggest to reconsider the abundant use of the term continuous.

We agree with this comment and have subsequently changed all instances of "continuous" to "quasi-continuous" to indicate that the spectra are indeed comprised of discrete measurements or, where appropriate, used a different adjective to better describe the data.

p. 5081, l. 21: actually typically these indices use fairly narrow wavebands, even from satellite platforms

From our understanding, various satellite platforms vary in the bandwidth used to calculate these metrics; however we have deleted “broad-band” from this sentence to reflect the variability in wavebands width from various platforms.

p. 5084, l. 1-23: is this paragraph truly necessary – we will anyhow learn later what the authors did to address the four questions

We believe that outlining the work within the Introduction immediately following the key Research Questions will help the reader to understand the logic for our Methods that follow.

p. 5088, l. 12: presumably you also applied a coordinate rotation to the wind data
Yes, we have added the coordinate rotation to the list of corrections applied to the raw data.

p. 5088, l. 25 and 26: net release and net uptake – uptake and release may be operating at the same time, eddy covariance however only allows measuring the net flux
Eddy covariance measures the net flux, but we separate uptake (GPP) from release (Reco) by standard methods described in Methods section 2.3 and at length in Knox et al (2014) and Hatala et al (2012), so we feel justified in using the partitioned “uptake” GPP fluxes for our analysis.

Table 1 and 2: GPP and NEE have different units at instantaneous and other time scales – correct? If so this should be noted in the table legend

Yes, we have added this information to the Table 1 and 2 legends.

p. 5099, l. 5-7: rather than representativity, isn’t the issue more that the reflection by the white flowers confounds the signal?

We believe that both the increased spatial variability at the Pasture compared to the Rice, in addition to the white flowers of the canopy, can contribute to a lower predictive power of the reflectance spectrum at this site.

p. 5099, l. 12: an UAV might be an appropriate tool for sampling the flux footprint
Yes, we have added this to the list of possible improvements to footprint sampling.

p. 5102, l. 14: if I am not mistaken, MODIS (Terra and Aqua) yield daily data, which are aggregated into the 8-day GPP product

Yes, thank you for this important correction and we have modified the manuscript accordingly.

177 **List of changes:**

- 178 1. Added Table 3, Supplementary Table 1.
- 179 2. Added Methods Section 2.5 and Results Section 3.4 to explain and present results from
- 180 the analysis of SVIs in comparison with PLSR modeling.
- 181 3. Minor edits to text and citation additions as described above in the Review Response.

182 **Predicting landscape-scale CO₂ flux at a pasture and rice paddy with long-term**
183 **hyperspectral canopy reflectance measurements**

184

185 Jaclyn Hatala Matthes^{1*}, Sara H. Knox², Cove Sturtevant², Oliver Sonnentag³, Joseph
186 Verfaillie², Dennis Baldocchi²

187

188 ¹Dept. Geography, Dartmouth College, 6017 Fairchild, Hanover, NH, USA

189 ²Dept. Environmental Science, Policy, and Management, University of California – Berkeley,
190 Berkeley, CA, USA

191 ³Dépt. Géographie, Université de Montréal, Montréal, Canada

192 * Corresponding Author: jaclyn.h.matthes@dartmouth.edu

193 **Abstract**

194 Measurements of hyperspectral canopy reflectance provide a detailed snapshot of
195 information regarding canopy biochemistry, structure and physiology. In this study, we collected
196 five years of repeated canopy hyperspectral reflectance measurements for a total of over 100 site
197 visits within the flux footprints of two eddy covariance towers at a pasture and rice paddy in
198 Northern California. The vegetation at both sites exhibited dynamic phenology, with significant
199 inter-annual variability in the timing of seasonal patterns that propagated into inter-annual
200 variability in measured hyperspectral reflectance. We used partial least-squares regression
201 (PLSR) modeling to leverage the information contained within the entire canopy reflectance
202 spectra (400-900nm) in order to investigate questions regarding the connection between
203 measured hyperspectral reflectance and landscape-scale fluxes of net ecosystem exchange (NEE)
204 and gross primary productivity (GPP) across multiple timescales, from instantaneous flux to
205 monthly-integrated flux. With the PLSR models developed from this large dataset we achieved a
206 high level of predictability for both NEE and GPP flux in these two ecosystems, where the R^2 of
207 prediction with an independent validation dataset ranged from 0.24 to 0.69. The PLSR models
208 achieved the highest skill at predicting the integrated GPP flux for the week prior to the
209 hyperspectral canopy reflectance collection, whereas the NEE flux often achieved the same high
210 predictive power at the daily- through monthly-integrated flux timescales. The high level of
211 predictability achieved by PLSR regression in this study demonstrated the potential for using
212 repeated hyperspectral canopy reflectance measurements to help partition NEE measurements
213 into its component fluxes, GPP and ecosystem respiration, and for using quasi-continuous
214 hyperspectral reflectance measurements to model regional carbon flux in future analyses.

215

Jaclyn Matthes 7/16/2015 11:08 AM

Deleted: continuous

217 1. Introduction

218 The development of remote sensing tools that bridge the scale of carbon flux
219 measurements from individual eddy covariance towers to broader, continuous spatial scales has
220 long been a goal of the earth systems science community (Bauer, 1975; Running et al., 1999;
221 Ustin et al., 2004). This goal inspired the formation of the international research group SpecNet,
222 developed to synthesize the collection of near-surface ground reflectance measurements at eddy
223 covariance tower sites to provide a crucial link between the spatial scales of eddy flux towers and
224 aircraft or satellite measurements (Gamon et al., 2010). Previous work in near-surface remote
225 sensing has demonstrated that normalized canopy reflectance indices can yield important insights
226 for understanding landscape-scale CO₂ flux measurements, particularly for understanding
227 patterns in CO₂ uptake through photosynthesis (Gamon et al., 1997; Inoue et al., 2008). Recent
228 work has also demonstrated the utility of using the entire reflectance spectrum to uncover new
229 normalized near-surface reflectance indices that are correlated with ecosystem productivity and
230 can be used to monitor canopy phenology with relatively inexpensive LED sensors (Ryu et al.,
231 2010a). Metrics based on canopy reflectance can be used as proxies for biological processes at
232 the surface when those biological processes have corresponding features that change the
233 reflectance and absorption of energy in the plant canopy. The two most commonly used remote
234 sensing metrics, the normalized difference vegetation index (NDVI) and the enhanced vegetation
235 index (EVI), track ecosystem productivity by measuring energy absorption at the visible
236 wavelengths where chlorophyll is active and comparing that to the reflectance or emission at
237 near-infrared wavelengths where active plant canopies dissipate energy (Liu and Huete, 1995;
238 Rouse et al., 1974). NDVI and EVI are widely used metrics since they can be calculated
239 worldwide (although at coarse spatial resolution of about 250m) by reflectance measurements

Jaclyn Matthes 7/16/2015 11:08 AM

Deleted: broad-band

Jaclyn Matthes 7/16/2015 11:08 AM

Deleted: (Liu and Huete, 1995; Rouse et al., 1973).

243 from the Moderate-Resolution Imaging Spectroradiometer (MODIS) instruments. The
244 widespread use of normalized indices has revolutionized the predictive power of global carbon
245 flux measurements, as they act as important proxies for photosynthetic carbon dioxide uptake in
246 plants that can be modeled through temporally quasi-continuous satellite imagery (Justice et al.,
247 1985; Potter et al., 1993; Running and Nemani, 1988; Tucker et al., 1985).

248 While these normalized indices have wide utility for predicting landscape-scale carbon
249 flux at spatial scales from that of near-surface sensors to satellite remote sensing, these indices
250 necessarily leave out much of the information provided within the entire visual and near-infrared
251 spectrum of canopy reflectance. Modeling techniques such as partial least-squares regression
252 (PLSR) (Wold et al., 2001) that can leverage the entire information contained within the quasi-
253 continuous canopy reflectance spectrum by reducing the regression variables to a set of fewer
254 latent variables (i.e. modeled variables that capture information from many individual regression
255 variables at once) are now widely used to predict traits at the leaf, plot, and canopy level.
256 Hyperspectral reflectance measurements have been used with PLSR methods to successfully
257 predict leaf-level traits like nitrogen (N) and carbon content, specific leaf area, protein, cellulose,
258 and lignin content, and even leaf isotopic ¹⁵N content and V_{max}, the maximum rate of
259 carboxylation during photosynthesis (Asner and Martin, 2008a; Bolster et al., 1996; Serbin et al.,
260 2012, 2014). PLSR has also been used with near-surface canopy hyperspectral reflectance
261 measurements to predict biomass and nitrogen content in wheat crops (Hansen and Schjoerring,
262 2003) and to predict pasture forage quality (Kawamura et al., 2008). Airborne hyperspectral
263 reflectance measurements have been used with PLSR to map canopy-level chemistry (Ollinger et
264 al., 2002; Smith et al., 2002), to predict citrus yields in orchards (Ye et al., 2009), and to map
265 floristic gradients in grasslands (Schmidt et al., 2007) and species diversity in tropical forests

Jaclyn Matthes 7/16/2015 11:08 AM

Deleted: continuous

Jaclyn Matthes 7/16/2015 11:08 AM

Deleted: a

268 (Asner and Martin, 2008b). This large range of studies across a diverse set of spatial scales, from
269 the leaf- to canopy-level, demonstrates the utility of using hyperspectral reflectance
270 measurements in conjunction with PLSR methods to increase the predictive power of remote
271 sensing relationships with ecological variables compared with traditional normalized indices.
272 Despite the proven utility of PLSR methods over a wide range of spatial scales, to our
273 knowledge no studies have yet investigated the potential for using hyperspectral reflectance
274 measurements to directly predict landscape-scale carbon fluxes through PLSR modeling.

Jaclyn Matthes 7/16/2015 11:08 AM

Deleted: continuous

275 The goal of this analysis was to investigate the ability of repeat canopy hyperspectral
276 reflectance to directly predict landscape-scale carbon dioxide (CO₂) fluxes at two short-
277 structured plant canopies. We measured replicated near-surface hyperspectral canopy reflectance
278 on 100 different sampling dates over the course of five years from 2010-2014 within the flux
279 footprint of two nearby eddy covariance tower sites with similar structure but different canopy
280 phenology in Northern California. The first site was a pasture where grasses grew over the winter
281 and the invasive pepperweed plant (*Lepidium latifolium*) was active throughout the summer. The
282 second site was an irrigated rice paddy with a simple phenology, where rice plants were present
283 only from May through October following the typical growing season pattern for agricultural
284 crops within this region. We combined the rich information contained within these repeated
285 hyperspectral canopy reflectance measurements with PLSR methods to predict landscape-scale
286 patterns in net CO₂ flux (net ecosystem exchange; NEE) and CO₂ uptake through canopy
287 photosynthesis (gross primary productivity; GPP).

288 We used this five-year long-term dataset of near-surface hyperspectral canopy reflectance
289 measurements collected at two sites in conjunction with landscape-scale eddy covariance CO₂
290 fluxes to answer the following four research questions:

- 292 1) How does canopy hyperspectral reflectance vary seasonally and inter-annually within and
293 across sites during different phenological stages?
- 294 2) How well can the [quasi](#)-continuous 400-900nm canopy reflectance spectrum predict GPP
295 and NEE at the two sites?
- 296 3) Are there significant differences in the ability to predict GPP and NEE at the pasture site
297 compared with the rice paddy?
- 298 4) At what timescale are fluxes most strongly correlated with changes in measured
299 hyperspectral canopy reflectance?

300 First, we examined the variability in measured hyperspectral reflectance within each site and
301 between the two sites on individual sampling dates and across years. This provided insight into
302 the dynamic nature of the canopy reflectance spectrum at these two study sites. The second two
303 questions addressed the ability of the hyperspectral reflectance spectra to capture changes in GPP
304 and NEE at the two sites, and tested whether the predictive power of hyperspectral reflectance
305 modeling with PLSR is higher at the rice paddy site, where GPP and ER are more closely
306 coupled than at the pasture, where GPP and ER are more decoupled due to different
307 environmental drivers (Hatala et al., 2012; Knox et al., 2014). The final research question
308 investigated the temporal scale at which the measured hyperspectral canopy reflectance
309 integrated previous CO₂ fluxes. The canopy traits that control hyperspectral reflectance (e.g.
310 chlorophyll, nitrogen, and water content in leaves, leaf abundance, etc.) are the emergent,
311 integrated response to previous ecophysiological variability. We tested the ability of the canopy
312 reflectance to predict instantaneous fluxes, and daily-, weekly-, and monthly-integrated carbon
313 fluxes at each of the sites to quantify the timescale at which the canopy reflectance integrated
314 prior ecophysiology, providing insight into the system memory of canopy reflectance. These

315 three integrated flux timescales represented the peaks in temporal autocorrelation due to daily
316 fluctuations in the diurnal cycle of plants and solar radiation, weekly fluctuations in synoptic
317 weather fronts, and monthly variability due to seasonal and phenological patterns, respectively
318 (Baldocchi et al., 2001b; Stoy et al., 2009). Together, these research questions yielded key
319 insights into the utility and limitations of using repeated hyperspectral canopy reflectance
320 measurements to predict landscape-scale CO₂ fluxes.

321

322 2. Methods

323 2.1 Site Characteristics

324 We collected replicated hyperspectral ground reflectance measurements of plant canopies
325 at two sites in Northern California with similarly structured, yet phenologically different, plant
326 canopies. The first site was a drained peatland pasture (hereafter referred to as “Pasture”) located
327 on Sherman Island in the Sacramento-San Joaquin Delta (latitude: 38.0373; longitude: -
328 121.7536; elevation: -4m) with annual grasses growing during the winter and spring, and the
329 invasive perennial pepperweed plant (*Lepidium latifolium*) active from spring through autumn
330 (Figure 3). Pepperweed produces a dense canopy of white flowers each year from about the
331 beginning of June through the end of August, creating increased complexity in canopy
332 reflectance during this time (Sonnentag et al., 2011a, 2011b). The second site was a rice paddy
333 (hereafter referred to as “Rice”) located on Twitchell Island in the Sacramento-San Joaquin Delta
334 (latitude: 38.1055, longitude: -121.6521, elevation: -5m) with an active growing season from
335 May through October and maintained as a fallow and flooded field for the remainder of the year
336 (Figure 3).

Jaclyn Matthes 7/16/2015 11:08 AM

Deleted: .

Jaclyn Matthes 7/16/2015 11:08 AM

Deleted: .

339 The two sites were located within 10km of each other in the Sacramento San-Joaquin
340 Delta, and as such, they experienced the same Mediterranean climate with hot and dry summer
341 months and rainy, cool winters. The 30-year mean annual air temperature (1981-2010) recorded
342 at a nearby climate station in Antioch, CA was 16.4°C, and mean annual precipitation was
343 335mm. Despite their similar climatology, the difference in hydrological and agricultural
344 management between the two sites results in ecosystems with plant canopies that are quite
345 different in phenology (Hatala et al., 2012; Knox et al., 2014). The water table at the Pasture was
346 maintained at a level always below the soil surface at around 50-80cm throughout the year.
347 While the phenology of grasses at the Pasture peaked during the springtime, the pepperweed
348 plants at the site remained relatively active throughout the summer as their roots can tap the
349 shallow water table, creating a biologically active canopy almost year-round (Sonnentag et al.,
350 2011a). The Rice was planted and flooded through irrigation management during the summer
351 growing season only, and the plant canopy sustained high rates of productivity during the
352 precipitation-free summer months. The field remained fallow and flooded during the remainder
353 of the year. Differences in the canopy phenology at both sites propagated into differences in the
354 peak periods of photosynthesis, where peak GPP at the Pasture occurs April-May and peak GPP
355 at the rice occurs August-September (Hatala et al., 2012; Knox et al., 2014).

356 ***2.2 Hyperspectral canopy reflectance sampling***

357 At both the Pasture and Rice, hyperspectral canopy reflectance was collected with a fiber
358 optic spectrometer (USB 2000; Ocean Optics, Dunedin, FL) with a detector range from 200-
359 1100nm at a height of 1m above the mean canopy surface. The fiber optic sensor was filtered
360 through a cosine corrector (CC-3-UV-S Spectralon) to ensure that the bi-hemispherical
361 reflectance from the ground surface was measured at an angle normal to the sensor surface

(Nicodemus et al., 1977; Schaepman-Strub et al., 2006). [We measured bi-hemispherical reflectance to minimize the contribution of background soil surfaces to the spectral signal, and we ensured that our reflectance signal was not comprised by low Sun zenith angles by sampling near midday \(Meroni et al., 2011\).](#) For this analysis we constrained our data to 400-900nm due to large levels of noise at the detection edges of this instrument. The spectrometer was mounted on a tripod approximately one meter above the canopy and was connected via USB cable to a laptop computer running the OOBBase32 software (USB 2000; Ocean Optics, Dunedin, FL) to capture spectra, which internally corrected for instrument-specific calibration parameters. Each field spectrum was collected and saved by OOBBase32. At the start of each site visit, the integration time within OOBBase32 was adjusted to the ambient light conditions and a reference dark spectrum measurement was collected by covering the fiber optic head with two layers of black electrical tape and orienting the sensor downward. at a height of 1m above the mean canopy surface bi-hemispherical (Nicodemus et al., 1977; Schaepman-Strub et al., 2006)

After this initial set-up, we collected a reflectance spectrum for each site replicate by first pointing the spectrometer directly skyward to record the spectrum of incoming energy, and within seconds, pointing the spectrometer directly at the ground surface to record the spectrum of reflected energy. Thus, we calculated the canopy reflectance for each replicate as the reflected spectrum normalized by the incoming spectrum. For each collection date at each site, we averaged the replicate spectra for this analysis to compute a single mean spectral reflectance per date at each site. The spectrometer records data at approximately 0.28nm intervals, and we smoothed each reflectance spectrum using a spline fit to 1nm intervals between 400-900nm in order to reduce instrumental noise in the data.

384 We measured canopy hyperspectral reflectance from July 2010 through September 2014
385 at both sites, collecting measurements during the entire year at the Pasture and during the
386 growing season at the Rice, which amounted to 100 total sampling dates at the Pasture and 71
387 total sampling dates at the Rice (Figure 1). On each sampling date, hyperspectral reflectance
388 measurements were collected at each site with a spatial and temporal replicate frequency suited
389 to the individual site heterogeneity. At the Pasture, where the canopy was spatially and
390 temporally heterogeneous, we measured hyperspectral reflectance approximately weekly, bi-
391 weekly, or monthly, with nine replicate canopy reflectances randomly sampled per visit. At the
392 Rice, which had lower spatial variability, hyperspectral reflectance was collected weekly or bi-
393 weekly during the growing season, with five replicate canopy reflectance spectra collected per
394 visit. We occasionally collected up to ten additional replicates at each of the sites, in order to
395 ensure that our smaller sampling sizes were capturing broad landscape-scale patterns in spatial
396 heterogeneity. At each site we randomly sampled canopy reflectance at locations approximately
397 10-20m within the flux tower footprint, the area most representative of the half-hourly flux
398 measurements. For partial least-squared regression analysis, we averaged across the
399 hyperspectral canopy reflectance replicates for each site and day. Because leaf geometry and
400 clumping can critically impact the interpretation of canopy reflectance measurements (Colwell,
401 1974), these two sites provide a useful first-case study for directly connecting hyperspectral
402 canopy reflectance measurements to CO₂ flux because both ecosystems have an erectophile in
403 leaf angle distribution for the majority of the year, minimizing shadow effects when field spectra
404 are collected near solar noon.

405 ***2.3 CO₂ flux measurements***

Both sites are active AmeriFlux and FLUXNET sites (Baldocchi et al., 2001a) measuring fluxes of energy, water vapor, and CO₂ using standard eddy covariance methods and processing procedures described elsewhere in detail (AmeriFlux site codes: US-Snd and US-Twt; Hatala et al., 2012; Knox et al., 2014; Sonnentag et al., 2011a). The eddy covariance technique was used to measure the fluxes of CO₂ at each site by collecting simultaneous 10 Hz measurements of vertical turbulence (w , m s⁻¹), measured with a sonic anemometer (Gill WindMaster Pro; Gill Instruments Ltd, Lymington, Hampshire, England), and CO₂ density (c , μmol m⁻³), measured with an infrared gas analyzer (LI-7500; Li-Cor Biosciences, Lincoln, NE). From these measurements we calculated the net half-hourly mean flux of CO₂ (NEE, μmol m⁻² s⁻¹) between the surface and atmosphere by averaging the covariance between w and c over a half-hourly time period after applying [a coordinate rotation and](#) a set of standard air density and temperature corrections (Detto et al., 2010; Schotanus et al., 1983; Webb et al., 1980). To partition NEE into gross primary photosynthesis (GPP, μmol m⁻² s⁻¹) and ecosystem respiration (ER, μmol m⁻² s⁻¹), net CO₂ fluxes were first gap-filled using artificial neural network (ANN) techniques outlined in detail within Knox *et al.* [2014], driven by meteorological variables (Moffat et al., 2007; Papale et al., 2006). After the net CO₂ fluxes were gap-filled using the ANN technique, we separated the net flux into GPP and ER by modeling nighttime NEE measurements as ER, since GPP is assumed to be zero at night (Reichstein et al., 2005). We prescribed the nighttime temperature dependence of ER by an Arrhenius-type model (Lloyd and Taylor, 1994), and extrapolated this model to the daytime, calculating GPP as the difference between NEE and modeled ER. Net CO₂ flux data within this analysis are presented from the atmospheric convention, where a negative flux indicates ecosystem uptake, and a positive flux indicates release from the ecosystem to the atmosphere.

429 Within this analysis we examined the predictive power of hyperspectral canopy
430 reflectance to explain patterns in instantaneous and daily-, weekly-, and monthly-integrated NEE
431 and GPP flux. We tested these variables separately in order to determine whether the canopy
432 reflectance better predicted an instantaneous flux measurement at the time of collection, or a flux
433 signal integrated over the previous day, week, or month. For instantaneous NEE and GPP flux,
434 we matched the time of spectral collection with the nearest mean half-hourly flux measurement,
435 where these values are presented in units of $\mu\text{mol m}^{-2} \text{s}^{-1}$. For the daily-, weekly-, and monthly-
436 integrated NEE and GPP fluxes, we integrated the net CO_2 and GPP flux over the course of the
437 previous day, week, or month for the date of spectral reflectance collection, where these values
438 are presented in units of $\text{g-C m}^{-2} \text{time}^{-1}$. For reference regarding the magnitude and temporal
439 dynamics of CO_2 fluxes at the Pasture and Rice, the instantaneous GPP flux and daily NEE flux
440 for both sites are plotted as Figure 2.

441 ***2.4 Partial Least-Squares Regression Modeling***

442 Partial least-squares regression is a standard method in chemometrics for modeling the
443 ability of a set of [quasi](#)-continuous spectral variables to predict a single response (Wold et al.,
444 2001). In this analysis we used PLSR methods with the hyperspectral canopy reflectance dataset
445 to model the response of instantaneous or integrated NEE or GPP. PLSR is similar to principle
446 components analysis (PCA), in that the modeling algorithm reduces a large predictor matrix of
447 spectral reflectance data to a reduced set of latent variables. In our study, the large predictor
448 matrix is the measured hyperspectral reflectance at each wavelength between 400-900 nm during
449 each sampling event, which in our analysis was reduced to a maximum of 10 latent variables that
450 contained the most significant sets of variables from the larger matrix for predicting
451 instantaneous or integrated NEE or GPP. PLSR typically outperforms PCA or standard step-wise

linear regression for situations where there is high co-linearity within the predictor matrix, such as within narrow-band spectral reflectance and chemometrics (Wold et al., 2001). For this analysis we used the PLS package (Mevik et al., 2013) within the R statistical environment (R Development Core Team 2014). All the R code used to conduct this analysis is freely available on GitHub at http://github.com/jhmatthes/canreflectance_flux_plsr.

For PLSR model fitting and validation, our methods followed those of Serbin *et al.* (2014), which used PLSR regression modeling to determine the ability of hyperspectral reflectance data to predict a suite of leaf traits. However, in this analysis, we used repeated measurements to examine how well the repeated hyperspectral reflectance measurements could directly predict landscape-scale fluxes of NEE and GPP. We conducted one set of PLSR regression modeling for the entire spectral reflectance dataset that combined both the Pasture and Rice data, and then two additional PLSR modeling exercises with the only the Pasture data and only the Rice data, to examine whether there were significant differences between the two sites in the resulting PLSR models. For each of the three PLSR modeling exercises, we split the data into model calibration (80% of the data) and independent validation (20% of the data; hereafter referred to as “Independent Validation”), where the model calibration data were used to fit the model, and the independent validation data were used to evaluate the ability of the model to predict landscape-scale NEE and GPP outside of the PLSR model fitting exercise. As in Serbin *et al.* [2014], we randomly split the model calibration data into 70% for model fitting (hereafter referred to as “Calibration”) and 30% for model uncertainty evaluation (hereafter referred to as “Evaluation”) over 1000 iterations to evaluate the uncertainty in PLSR model development. So overall, we used 56% of the total data for Calibration, 24% of the data for Evaluation, and an unchanging 20% of the data for Independent Validation to test the predictive power of the final

mean models. We conducted an initial optimization with a single set of Calibration data and Evaluation data to determine the total number of PLSR latent variables to include in each model by minimizing the prediction residual sum of squares, calculated through leave-one-out cross-validation (Chen et al., 2004). We used the entire 400-900nm spectrum range with these PLSR methods to fit the instantaneous and daily-, weekly-, and monthly-integrated NEE and GPP flux data.

To quantify the performance of each PLSR model we calculated the coefficient of determination (R^2), the root mean square error (RMSE), and the model bias. We used the 1000 iteration bootstrapping approach for each PLSR to quantify the model calibration performance as in Serbin *et al.* [2014]. From the random 70% to 30% split of the Calibration and Evaluation data, we generated new estimates for each iteratively removed sample. This allowed us to test the stability and generality of the models using different sets calibration data and to estimate robust errors for the prediction of flux measurements by representing the uncertainty across measurements, spectral data, and the PLSR modeling approach. For each set of 1000 modeling iterations over the random calibration/validation fit dataset split, we calculated the resulting mean PLSR model coefficients and the variable importance of projection (VIP) score associated with the reflectance measured at each wavelength. The VIP score represents the statistical contribution of each individual wavelength to the overall fitted PLSR model across all latent model components. In this way, the VIP score can be used to identify the wavelengths that contribute the most information for predicting the variable at hand (in this case, either NEE or GPP). Using the mean of the bootstrapped PLSR models, we tested each final mean model against the 20% of original data left aside for Independent Validation by linear regression.

2.5 Standardized vegetation indices for GPP and NEE prediction

We analyzed the skill of standardized vegetation indices (SVIs) in predicting NEE and GPP flux at the Pasture and Rice, and compared the utility of these models to our PLSR modeling results. Due to their wide use in other studies, we tested the normalized difference vegetation index (NDVI; $[R_{800} - R_{680}] / [R_{800} + R_{680}]$; Rouse et al., 1974), NDVI calculated with the wavelengths from the Moderate Resolution Imaging Spectroradiometer satellite (NDVI_{MOD}; $[R_{841-876} - R_{620-670}] / [R_{841-876} + R_{620-670}]$), green NDVI (NDVI_g; $[R_{800} - R_{550}] / [R_{800} + R_{550}]$; Gitelson et al., 1996), red-edge NDVI (NDVI_{re}; $[R_{800} - R_{700}] / [R_{800} + R_{700}]$; Gitelson and Merzlyak, 1994), and the photochemical reflectance index (PRI; $[R_{531} - R_{570}] / [R_{531} + R_{570}]$; Gamon et al., 1992), where R indicates reflectance in the subscripted wavelengths in nanometers. For all SVIs except NDVI_{MOD}, we averaged the measured reflectance for a 10nm window centered on the reflectance value to reduce measurement noise.

We assessed the ability of SVI measurements to predict NEE and GPP fluxes for All data, the Rice only, and the Pasture only by randomly selecting 80% of the reflectance spectra for calibration, leaving 20% of the data for prediction. For GPP fluxes, we assessed the fit and prediction of SVIs with a log-linear model as this model best fit the data, and for NEE we used a simple linear model, which fit the data better than a log-linear model. To assess the ability of the SVIs to predict GPP and NEE, we performed an iterative calibration/prediction analysis where we randomly parsed the data into 80% calibration and 20% prediction for 100 iterations, and present the mean statistics for comparative analysis with the PLSR modeling results.

3. Results

3.1 Spatiotemporal variability in hyperspectral canopy reflectance

520 There was significant seasonal, inter-annual, and site-level variability across the
521 hyperspectral canopy reflectance measurements collected over the course of five years at both
522 sites. Intra-site variability within canopy reflectance changed due to the phenological stage of the
523 ecosystem, whereas inter-annual variability was driven by changes in the timing of these
524 phenological events. The Pasture tended to be more spatially heterogeneous than the Rice,
525 observed through the higher intra-site variability during an individual sampling event,
526 particularly in the infrared reflectance (Figure 3). This intra-site variability at the Pasture is
527 caused by higher spatial heterogeneity in canopy structure compared with the Rice, which is a
528 monoculture with a simpler crop phenological cycle. During the green leaf-out stage at both the
529 Pasture and Rice, the patterns of hyperspectral reflectance were quite similar, with a peak at the
530 green wavelengths, absorption in the red wavelengths, and high reflectance in the near-infrared
531 wavelengths (Figure 3a,b). Intra-site variability across the spectrum was high across at the
532 Pasture during periods of white pepperweed flowering that produced a much higher albedo than
533 the green canopy and obscured reflectance patterns in the green and red wavelengths, despite
534 relatively high plant productivity during this time (Figure 3c). The closest analogous
535 phenological stage to this period at the Rice was during the time at which the rice has seeded and
536 the plants have dried in preparation for harvest, when the Rice experienced similar trends in
537 increased albedo through the visible wavelengths (Figure 3d). However, the magnitude of the
538 senescing Rice reflectance was not as large as the white pepperweed canopy at the Pasture, and
539 in addition the reflectance spectra were not obfuscated during this time since the rice
540 productivity was quite low at this point in the growing season.

541 The seasonal and inter-annual patterns in narrow-band reflectance in the green (550 ± 5
542 nm), red (640 ± 5 nm), and near-infrared (NIR; 800 ± 5 nm) wavelengths also highlighted intra-site

543 and inter-annual variability. At the Pasture, there was low intra-site variability and inter-annual
544 variability in green reflectance from January through the end of May, when the grass canopy was
545 present at the site (Figure 4a). However, when pepperweed became the dominant canopy plant at
546 the Pasture during the summer growing season, both replicate and inter-annual variability
547 increased as the pepperweed created a more heterogeneous cover than the grass due to its white
548 flowers and more spatially variable structure than the winter grass canopy. The same pattern was
549 evident in the red reflectance at the Pasture, with low variability in the second half of winter and
550 spring, and a large increase in variability during the summer growing season and autumn (Figure
551 4c). At the Rice, there was also large inter-annual variability in the timing of the seasonal pattern
552 green and red reflectance, however there was a more discernible seasonal pattern of reflectance
553 that tracks within years across the entire growing season (Figures 4b,d). For example, each year
554 green reflectance and red reflectance started high, decreased as the growing season progressed,
555 then eventually increased again as the rice straw dried before harvest. The NIR reflectance at the
556 Pasture had a stable mean through the year with little inter-annual variability but large intra-site
557 variability across the year (Figure 4e). The Rice NIR reflectance had a consistent seasonal
558 pattern between years, with low reflectance in the early growing season and increasing NIR
559 reflectance as the canopy developed due to the change in the rice canopy closure as the growing
560 season progressed (Figure 4f). Although there was a consistent phenological trend in NIR
561 reflectance at the Rice each year, there remained inter-annual variability in the timing of the NIR
562 minimum and larger intra-site variability compared with reflectance in the visible wavelengths.

563 ***3.2 Calibrated PLSR models for predicting NEE and GPP***

564 We fit PLSR models to the hyperspectral data to predict landscape-scale NEE and GPP at
565 four integrated flux timescales: instantaneous flux measurements, and daily-, weekly-, and

566 monthly-integrated flux measurements for the period preceding the time of hyperspectral canopy
567 reflectance collection. In this analysis we determined the optimal number of latent variables to
568 include for each model by minimizing the predictive residual sum of squares. The number of
569 optimal latent variables included in the PLSR models ranged from 2-8, which indicated that
570 some models could achieve the best predictive statistical fit for NEE and GPP with a much lower
571 number of components than other models (Table 1). For the PLSR models that included the
572 entire canopy reflectance dataset for both sites, the optimal number of latent variables was stable
573 at six components, except for the instantaneous GPP model, which included seven components.
574 The number of optimal components was more variable across the PLSR models for the Pasture
575 reflectance data (2-8 components) compared with those from the Rice reflectance data (4-6
576 components).

577 As expected, across all models, the R^2 for the PLSR Calibration was higher than the R^2
578 for the PLSR Evaluation fit, and the RMSE was lower for the Calibration and higher for the
579 Evaluation during the model calibration step (Table 1). The fit statistics presented within Table 1
580 show the mean fit statistics for the 1000 iterations of random 70% Calibration, 30% Validation
581 data selection from the 80% total data used during the model development fitting process. For
582 each PLSR model, the 1000 iterated fit statistics followed a normal distribution with low
583 variance, which indicated only a low bias to selecting the Calibration and Evaluation data so only
584 the mean results are presented within Table 1. Across almost all of the CO₂ flux prediction
585 variables, the PLSR models for the Rice dataset achieved the highest fit for both the Calibration
586 ($R^2 = 0.77$ - 0.92) and Evaluation ($R^2 = 0.58$ - 0.68) exercises, the PLSR models with the dataset
587 including both sites achieved a slightly lower overall fit for Calibration ($R^2 = 0.63$ - 0.87) and

588 Evaluation ($R^2 = 0.24-0.69$), and the PLSR models for the Pasture had the lowest overall fit for
589 Calibration ($R^2 = 0.38-0.97$) and Evaluation ($R^2 = 0.29-0.56$) (Table 1).

590 For each set of 1000 modeling iterations over the random calibration/validation fit dataset
591 split, we calculated the resulting mean PLSR model coefficients and the variable importance of
592 projection (VIP) statistic associated with each wavelength. Across all fitted PLSR models, as the
593 timescale of the fitted integrated flux increased from instantaneous to daily-, weekly-, and
594 monthly-integrated values, the VIP statistic in the visible wavelengths (400-700nm) decreased
595 and the VIP statistic in the near-infrared wavelengths (700-900nm) increased (Figure 5). This
596 indicated that for flux measurements on short timescales, the reflectance in the visible
597 wavelengths contributed the highest explanatory power to the PLSR model components, but at
598 longer timescales structural changes in the canopy that are correlated with the NIR range became
599 more important for predicting GPP and NEE flux. This pattern was especially apparent for the
600 VIP scores of the GPP model using the dataset with both sites (Figure 5a), where there was a
601 dramatic shift in VIP scores between the weekly- and monthly-integrated flux models. For the
602 weekly-integrated GPP flux model and those at shorter timescales, the highest VIP scores were
603 contributed by the visible wavelengths, with a peak in the red wavelengths near 700nm. However
604 for the monthly-integrated GPP flux model, there was a dramatic difference where the highest
605 VIP scores shifted from the visible to the NIR range, indicating that structural components of the
606 plant canopy correlated with NIR reflectance contributed higher predictive power than
607 reflectance in the visible part of the spectrum. There is a lower shift in VIP scores across
608 integrated flux timescales in the models developed with only the Rice dataset (Figure 5e-f)
609 compared against the models developed with only the Pasture dataset (Figures 5c-d), likely

reflecting the increased spatial and phenological complexity of the Pasture ecosystem compared with the relatively homogeneous Rice.

Across all models, the visible wavelengths that contributed the most information to the PLSR models, as determined by the magnitude of the VIP score, were within the red portion of the visible spectrum (Figure 5). Most PLSR models had VIP scores above 1.0 that correlated with reflectance at 642 and 662 nm, the wavelengths of chlorophyll absorption. Across most PLSR models there was also a peak in the VIP score near 673 nm, the wavelength of chlorophyll fluorescence. However, the second band of chlorophyll fluorescence at 726nm, exhibited low VIP scores across all models. For both of the PLSR models developed using only the Pasture dataset, there were also high VIP scores within the violet and blue range of the visible spectrum, from 400-450nm. These high VIP scores in the violet-blue portion of the spectrum could be partly explained by the chlorophyll a and b absorption peaks at 430nm and 460nm, because slightly higher VIP scores were also observed at the Rice site for these wavelengths (Figure 5e-f). However, this part of the spectrum at the Pasture site was particularly significant compared with the other models, and this could correspond to white reflectance of the pepperweed flowers at the site. When the pepperweed canopy was blooming, the bright white flowers reflected light across the entire visible spectrum, a unique characteristic to this site, where the high visible albedo in this spectral range might also have contributed to the high VIP scores within this portion of the spectrum (Figure 5c-d).

3.3 Independent Validation of PLSR models for NEE and GPP

After we fit the PLSR models to 80% of the entire dataset through 1000 iterations of different random sets of Calibration and Evaluation data, we tested the mean fitted models against the Independent Validation data (the 20% of the original dataset left out of the PLSR

633 model fitting process). In general, the fitted PLSR models achieved a good fit with the
634 measurements for this Independent Validation dataset, where the R^2 fit between the predicted
635 and actual NEE and GPP ranged from 0.26 to 0.69 (Table 2). As was the case for the calibration
636 and validation R^2 fits during the PLSR calibration process, the Rice dataset achieved the highest
637 R^2 values (0.40-0.69), the dataset with both sites achieved the second-highest set of R^2 (0.27-
638 0.62), and the Pasture dataset had the lowest R^2 (0.27-0.54). As in the previous discussion for the
639 Calibration and Evaluation fits to these three sets of data, we believe that the lower level of
640 predictability at the Pasture is due to the higher level of spatial heterogeneity and phenological
641 complexity compared with the Rice.

642 Although all models achieved a statistically significant fit between the predicted and
643 measured CO_2 fluxes with the Independent Validation dataset with relatively high R^2 values, the
644 uncertainty in the prediction was significantly lower for the models that included all the data
645 compared with the models that included only either the Pasture or Rice data. This pattern is
646 clearly observed within the Independent Validation fit for the daily GPP and NEE data (Figure
647 6). For the daily prediction of both GPP and NEE, the dataset that included all the data had a
648 smaller range for both the 95% confidence interval and 95% prediction interval for the
649 relationship between predicted and actual GPP and NEE. This trend likely represented an
650 increase in predictive power achieved by including a larger dataset with a wider range of values
651 both for NEE and GPP and for the measured hyperspectral reflectance. As the datasets that
652 included either the Pasture and Rice data only had a lower amount of data overall as well as a
653 narrower range of values, the confidence in the ability to predict NEE and GPP at these
654 individual sites was lower compared with the power of using the entire combined dataset.

655 | **3.4 Prediction of NEE and GPP fluxes with standardized vegetation indices**

We compared the ability of a suite of commonly used SVIs to predict GPP and NEE with the skill of the mean PLSR models developed within this study. Overall, the suite of NDVI SVIs performed reasonably well at predicting both GPP and NEE, and models tested with all the reflectance data for both sites achieved predictive R^2 values that ranged from 0.18 to 0.59 (Table 3; Supplementary Table 1), where red-edge NDVI was the SVI that achieved the highest skill for predicting GPP and NEE for the sites in this study. PRI was not well suited to predicting CO_2 fluxes at these sites, and models for this SVI achieved predictive R^2 fits that ranged from 0.02 to 0.22.

For models that fit all the data from both sites, the predictive fit from PLSR modeling outperformed the red-edge NDVI (the best-fit SVI) at the instantaneous and weekly timescales, the two models were not significantly different at the daily timescale, and red-edge NDVI outperformed PLSR modeling at the monthly timescale (Table 3). PLSR modeling outperformed SVIs across all timescales for models that fit the Pasture data only. The performance of red-edge NDVI and PLSR models were not significantly different at instantaneous, daily, and weekly timescales when fit with the Rice data only, however red-edge NDVI was a better predictor of monthly CO_2 fluxes than the PLSR models (Table 3).

3.5 Prediction of NEE and GPP fluxes across different timescales

We investigated the ability of PLSR modeling with the hyperspectral canopy reflectance measurements to predict instantaneous GPP and NEE fluxes from the same half hour of spectral measurement, in addition to fluxes integrated over the previous day, week, and month. Previous work determined that sampling errors in eddy covariance flux measurements diminished when the fluxes were integrated over the course of many days (Moncrieff et al., 1996). We expected that the instantaneous flux would achieve the lowest correlation with the measured canopy

reflectance since reflectance changes more slowly compared with CO₂ flux, and that the fluxes integrated over longer timescales would provide a stronger signal with a higher predictive capacity. For the Calibration and Evaluation during the initial PLSR model fitting, there was no strong evidence that one timescale (instantaneous, daily, weekly, or monthly flux) was particularly better fit with the hyperspectral canopy reflectance than the other timescales (Table 1). However, during the evaluation of the predictive power of the PLSR models with the Independent Validation data, most models achieved the highest predictive R² with GPP flux at the weekly-integrated timescale, and we found no clear optimal timescale for predicting NEE with measured hyperspectral reflectance data (Table 2; Figure 7).

4. Discussion

4.1 Sources of variability in measured reflectance

Variation across the measured hyperspectral canopy reflectance was dominated by inter-annual variability in the timing of canopy phenology (Figures 3,4). At the Rice, transitions were typical for an agricultural crop, where canopy reflectance incorporated portions of the background flooded soil in conjunction with the emerging green plants early in the growing season, with canopy closure achieved by early July (Beget and Di Bella, 2007). After flooding when the Rice canopy closed, there was less intra-site variability in measured reflectance, until the end of the growing season when the rice plants started to senesce and dry before harvest (Figure 4). At the Pasture, canopy phenology was more complicated, marked by a transition from a green grass canopy to a green pepperweed canopy in April, followed by the white flowering of the pepperweed canopy from June through August, which increased intra-site variability in measured reflectance (Figure 4). Both the Rice and Pasture experienced significant inter-annual

variability in the start and end dates of these phenological patterns, but despite this variability the sites experienced relatively low variability in the overall CO₂ flux (Figure 2). The primary driver of inter-annual variability at the Pasture was the timing of summer drought in the Mediterranean climate, and canopy management (Sonnentag et al., 2011a). These primary controls agreed with the results from European syntheses of FLUXNET sites where water was a key driver of inter-annual variability in NEE (Reichstein et al., 2007). At the Rice, inter-annual variability was driven by changes in the start and end dates of canopy phenology that were driven by changes agricultural management of the planting and harvesting dates each year and smaller changes in fertilizer management (Hatala et al., 2012; Knox et al., 2014). The timing of the planting and harvest at the Rice is controlled by logistical environmental drivers, as the field must be dry enough to drive farm equipment through the soil, and warm enough to ensure seedling survival. Differences in these variables from year to year created variability in the planting dates, and subsequent variability in the seasonal trajectory of hyperspectral canopy reflectance (Figures 3,4). There are also important differences between PLSR methods using the complete spectrum and standardized vegetation indices (SVIs) that may lead to differences in interpreting which bands are best suited for correlation with CO₂ fluxes. Because SVIs are normalized by a reference band, they may be better suited to reducing noise within temporal trends in reflectance time series, particularly at sites that experience a wide range of illumination conditions. While the PLSR methods used in this analysis benefit from the large information content that results from using the entire reflectance spectrum, the measurements represent relative reflectance values rather than normalized reflectance ratios, and thus likely include more noise in the measurement time series than SVIs. This is an important trade-off when considering whether to use the entire reflectance spectrum or SVIs to understand how canopy reflectance tracks CO₂

725 [fluxes, but the simple canopy structure at the sites in this analysis and the collection of](#)
726 [measurements during ideal illumination conditions limits the overall noise within the reflectance](#)
727 [time series.](#)

728 **4.2 Predicting NEE & GPP with PLSR models**

729 Along with the inter-annual variability experienced at both sites, there were also
730 differences in the intra-site variability of measured reflectance within the two flux tower
731 footprints. The Pasture site was more spatially heterogeneous than the Rice, driving increased
732 variability among replicate hyperspectral reflectance spectra at the site (Figure 4). The increased
733 spatial variability at the Pasture was reflected in the lower predictive power of the PLSR models
734 in predicting GPP and NEE with only the Pasture dataset (Tables 1,2). The lower overall fit
735 between the hyperspectral measurements and CO₂ flux at the Pasture can be explained through
736 [three](#) possible mechanisms: 1) the hyperspectral canopy reflectance measurements at the Pasture
737 are less representative of the entire flux footprint than the Rice data, 2) white pepperweed
738 flowers in the Pasture canopy during summertime create an obstruction for reflectance that
739 degrades the representativeness of measured spectra (Hestir et al., 2008; Sonnentag et al.,
740 2011b). [3\) the lack of irrigation at the Pasture compared with the Rice could create conditions of](#)
741 [water stress during which reflectance becomes temporally decoupled from CO₂ flux.](#) It is likely
742 that [all](#) of these factors contributed to the lower PLSR predictive power at the Pasture, and [in](#)
743 [particular](#) the obstruction by white canopy flowers presented a challenge that is somewhat
744 unavoidable for canopy reflectance studies in complex ecosystems. Changes to future sampling
745 efforts that address the footprint representativeness, for example increasing the number and
746 spatial distribution of hyperspectral reflectance collected at the Pasture [or flying an unmanned](#)

Jaclyn Matthes 7/16/2015 11:08 AM

Deleted: two

Jaclyn Matthes 7/16/2015 11:08 AM

Deleted: and/or

Jaclyn Matthes 7/16/2015 11:08 AM

Deleted: .

Jaclyn Matthes 7/16/2015 11:08 AM

Deleted: both

[aerial vehicle \(UAV\) with a mounted hyperspectral sensor](#), might help to further improve the future PLSR predictive power.

The most important wavelengths for the PLSR modeling with the GPP and NEE flux data in this study fell in line with previous work that has examined correlations between reflectance and traits of photosynthetic uptake (Main et al., 2011). However, we were initially surprised to find that the green wavelengths were not dominant components for prediction of either NEE or GPP across the suite of calibrated PLSR models (Figure 5). These results do parallel recent work in oak forests that demonstrated a temporal mismatch between peak greenness and peak leaf chlorophyll content (Yang et al., 2014). This temporal mismatch could be the cause for the insignificant correlation in narrow-band green reflectance, because at both sites vegetation is a lighter green early in the growing season and develops into a darker green as the season progresses. There were particularly high VIP scores in the blue visible wavelength range, from 400-450 nm, at the Pasture site (Figure 5c,d), which could be partly explained by the chlorophyll a and b absorption peaks at 430nm and 460nm since the Rice also experienced slightly higher VIP scores in this region (Figure 5e-f). However, the magnitude of the VIP scores in this region at the Pasture far exceeded those at the Rice. There are two possible explanations for this marked increase in the importance of the blue visible wavelengths at the Pasture: 1) white reflectance of the pepperweed flowers at the site could be increasing the albedo within this portion of the spectrum; 2) the more complex phenology at the site with annual grass and pepperweed senescence is periodically driving reflectance near 420 nm in response to these periods of stress (Carter and Miller, 1994). While the Pasture shifted toward much higher reflectivity across the visible wavelengths during the brief period of white flowering in late spring (Figure 3a), this site

773 also experienced more dynamic phenology overall, with browning of the grass in early summer
774 and of the pepperweed in late summer.

775 Almost all of the PLSR models predicting instantaneous and daily- and weekly-integrated
776 NEE and GPP had a peak in the VIP score at red wavelengths (Figure 5). Reflectance features
777 within this portion of the spectrum include absorption in the red wavelengths at 642 and 662 nm
778 correlated with chlorophyll absorption, and reflectance in the chlorophyll a fluorescence
779 wavelengths that occurs near 673 nm. The maximum VIP score in the visible wavelengths across
780 nearly all of the PLSR models occurred near the end of the red portion of the spectrum between
781 670-680 nm, indicating that these wavelengths provided critical information to the latent
782 variables that comprised most of the PLSR models (Figure 5). This result paralleled previous
783 work that demonstrated the importance of narrow-band reflectance at 670-680 nm for predicting
784 chlorophyll absorption features across a diverse suite of plant canopies (Carter and Miller, 1994;
785 Dawson et al., 1999; Gitelson and Merzlyak, 1997; Main et al., 2011).

786 The differences among the predictive power of the PLSR models that included all the
787 data compared with the models developed at individual sites highlighted important
788 considerations for future work in this area. The predictive models with the smallest 95%
789 prediction intervals originated from the models that included all of the data from both sites
790 (Table 2), demonstrating the power of using larger datasets, with a wider range of values, to
791 develop the predictive capacity of PLSR models. Further improvements in PLSR predictive
792 power might be achieved by building upon this data to include paired hyperspectral-eddy flux
793 datasets from additional sites that can expand and refine the connection between reflectance and
794 CO₂ flux. This approach has particular promise for sites with automated hyperspectral sensing
795 systems in conjunction with eddy covariance measurements ([Balzarolo et al., 2011](#); [Hilker et al.,](#)

2007; Leuning et al., 2006; Rossini et al., 2010). However, we do emphasize that changes in the canopy complexity and clumping are important consideration for such work at other sites, compared with the short-statured canopies with low clumping indices (Ryu et al., 2010b) included in this study. In canopies with more complex leaf and branch clumping, hyperspectral canopy reflectance measurements will need to be combined with radiative transfer modeling in order to accurately model the energy reflectance spectrum (Knyazikhin et al., 2013; Verhoef and Bach, 2007).

In testing the ability of common SVIs used in the literature to predict GPP and NEE, the skill of some NDVI models were on par with that of the PLSR models when developed using all the data from both sites or the Rice data only (Table 3). We believe that SVIs well-predicted GPP and NEE at the Rice due to its simple annual phenology and corresponding seasonal pattern in CO₂ flux. However, PLSR modeling significantly outperformed SVI models for predicting GPP and NEE flux when developed using only the Pasture data, due to the increased canopy complexity at the Pasture site. At the Pasture, the PLSR approach captured more variance within the dataset through its ability to model more complex relationships across the entire spectrum compared with SVIs, which focus only on two spectral areas. This highlights the improved utility for PLSR modeling compared with the use of SVIs to predict ecosystem CO₂ fluxes from canopies with complex phenological shifts.

4.3 CO₂ flux prediction at various timescales

Across all sets of PLSR models, there was an interesting shift in VIP scores from the visible wavelengths to the NIR wavelengths as the timescale of NEE and GPP integration increased (Figure 5). An increase in structural complexity drives higher NIR reflectivity (Main et al., 2011), and the VIP scores across the suite of PLSR models showed that this structural

Jaclyn Matthes 7/16/2015 11:08 AM

Deleted: (Balzarolo et al., 2011; Hilker et al., 2007; Leuning et al., 2006; Rossini et al., 2010)

822 components of the canopy driving NIR reflectance became increasingly important to predicting
 823 both NEE and GPP as the integrated timescale increased. This demonstrated that reflectance in
 824 visible wavelengths correlated with chlorophyll content was most important for short-term flux
 825 prediction, but canopy structural changes in the NIR wavelengths was most important for longer-
 826 term flux prediction. These results are analogous with those from a modeling study across a
 827 network of European grassland sites that found a strong correlation between GPP and NIR
 828 reflectance indicative of phenological shifts in structural canopy components independent of
 829 changes in chlorophyll reflectance (Balzarolo et al., 2015). An important constraint of our
 830 analysis is that the field spectrometer used only measured wavelengths up to 900 nm reliably,
 831 making analysis at longer wavelengths in the infrared area correlated with leaf structural
 832 components such as fiber, lignin, and cellulose content impossible (Serbin et al., 2014).
 833 However, this same approach of canopy-level PLSR modeling could be used in conjunction with
 834 a spectrometer capable of making wider spectral reflectance measurements at eddy covariance
 835 sites to evaluate longer wavelength areas of the short-wave IR (SWIR) spectrum, for example
 836 with the newly developed WhiteRef automated sensor for quasi-continuous SWIR hyperspectral
 837 measurements (Sakowska et al., 2015).

838 Comparing the predictive fit achieved with the PLSR models across different CO₂ flux
 839 timescales with the Independent Validation dataset provided important insights into the temporal
 840 scale of CO₂ flux integration represented by the hyperspectral canopy reflectance collection at a
 841 moment in time. Almost all of the final PLSR models achieved the highest predictive fit with the
 842 weekly-integrated GPP fluxes (Figure 7). The changes in the PLSR predictive power for NEE
 843 and GPP at different timescales provided important information for considering what exactly is
 844 represented by measured hyperspectral reflectance in the field, as canopy biochemistry is in fact

Jaclyn Matthes 7/16/2015 11:08 AM
 Deleted: An important constraint

Jaclyn Matthes 7/16/2015 11:08 AM
 Deleted: this

Jaclyn Matthes 7/16/2015 11:08 AM
 Deleted: NIR

Jaclyn Matthes 7/16/2015 11:08 AM
 Deleted: at longer wavelengths.

849 an emergent response to biological and environmental drivers that are integrated through time.
850 The fact that all three models achieved the best predictive fit with the Independent Validation
851 data for GPP at the weekly timescale yielded support for modeling efforts that determine carbon
852 fluxes from MODIS satellite reflectance, which is aggregated into an 8-day timescale. The
853 results of this flux timescale analysis are congruous with those from previous work, which found
854 a good correlation between gross CO₂ flux and the 8-day MODIS data timescale (Sims et al.,
855 2005). While there was a clear signal in the higher predictive power for estimating the weekly-
856 integrated GPP flux compared with other timescales, there was less consistency within the best
857 predictive timescale for estimating NEE (Figure 7). This is likely due to the fact that NEE is a
858 combination of both GPP and ER, which change on different timescales in response to different
859 environmental drivers and are more highly coupled at the Rice than they are at the Pasture
860 (Hatala et al., 2012; Knox et al., 2014). The fact that NEE achieved a good fit with canopy
861 hyperspectral reflectance through the monthly timescale for the models developed with all the
862 data (Figure 7a) could indicate that the system memory in carbon flux at these sites is integrated
863 over a longer timescale than was tested in this analysis, and that canopy biochemistry collected at
864 one moment reflects at least the previous month of integrated NEE flux.

865

866 5. Conclusions

867 This analysis demonstrated that using PLSR modeling with repeated near-surface
868 hyperspectral canopy reflectance created reliable predictive models of NEE and GPP flux for
869 two short-structured plant canopies with different phenology and significant intra-site and inter-
870 annual variability in canopy reflectance. The PLSR models developed from hyperspectral canopy
871 reflectance collected during 100 site visits from 2010-2014 at a Pasture and a Rice paddy

Jaclyn Matthes 7/16/2015 11:08 AM

Deleted: has

Jaclyn Matthes 7/16/2015 11:08 AM

Deleted: orbit time

Jaclyn Matthes 7/16/2015 11:08 AM

Deleted: overpass time

875 achieved a high level of predictability for both NEE and GPP flux where the predictive R^2
876 ranged from 0.24 to 0.69 using an independent validation dataset. The higher variability in
877 measured hyperspectral reflectance at the Pasture did decrease the predictive power of the PLSR
878 models when compared against those developed at the Rice site with a more homogeneous
879 canopy. The PLSR models were most skilled at predicting the GPP flux for the integrated week
880 prior to the collection of canopy reflectance. Although the use of PLSR methods with
881 hyperspectral field reflectance such as those presented within this analysis need to be rigorously
882 tested with a much larger dataset and in more diverse ecosystems, the results from this analysis
883 showed promise for using repeated hyperspectral canopy reflectance to directly predict
884 landscape-scale carbon flux. Use of this method, particularly if developed with large datasets
885 collected over several years, might help to constrain GPP estimates through the integration of
886 additional datasets into the modeling efforts that partition NEE into GPP and ER at flux sites
887 (Hilker et al., 2014). The development of PLSR models to predict NEE and GPP from
888 hyperspectral canopy reflectance collected within flux tower footprints is a promising avenue of
889 future research, particularly with the development and deployment of hyperspectral satellite
890 sensors such as NASA's Hyperspectral and InfraRed Imager (HyspIRI; [http://](http://hyspiri.jpl.nasa.gov)
891 <http://hyspiri.jpl.nasa.gov>), which will provide continuous spatial coverage of measured
892 hyperspectral reflectance.

893

894 **6. Author Contributions**

895 D.D.B., J.H.M., and O.S. designed the experiment, all co-authors collected, processed, and
896 analyzed the reflectance and eddy covariance measurements, J.H.M. designed and conducted
897 PLSR modeling, and J.H.M. wrote the manuscript with input from all co-authors.

898

899 **7. Acknowledgements**

900 The authors would like to thank Bryan Brock and the California Department of Water Resources
901 for funding through DWR contract 4600008849. This research was also supported by the United
902 States Department of Agriculture NIFA grant number 2011-67003-30371, and the National
903 Science Foundation Atmospheric and Geospace Science Program grant AGS-0628720. J.H.M.
904 thanks the National Science Foundation Graduate Research Fellowship program for support
905 through grant DGE-1106400.

906

907

908 8. Bibliography

- 909 Asner, G. and Martin, R.: Spectral and chemical analysis of tropical forests: Scaling from leaf to
910 canopy levels, *Remote Sens. Environ.*, 112(10), 3958–3970, doi:10.1016/j.rse.2008.07.003,
911 2008a.
- 912 Asner, G. P. and Martin, R. E.: Airborne spectranomics: mapping canopy chemical and
913 taxonomic diversity in tropical forests, *Front. Ecol. Environ.*, 7(5), 269–276,
914 doi:10.1890/070152, 2008b.
- 915 Baldocchi, D. D., Falge, E., Gu, L. H., Olson, R., Hollinger, D., Running, S., Anthoni, P.,
916 Bernhofer, C., Davis, K., Evans, R., Fuentes, J., Goldstein, A., Katul, G., Law, B., Lee, X. H.,
917 Malhi, Y., Meyers, T., Munger, W., Oechel, W., U, K. T. P., Pilegaard, K., Schmid, H. P.,
918 Valentini, R., Verma, S., Vesala, T., Wilson, K. and Wofsy, S.: FLUXNET: A new tool to study
919 the temporal and spatial variability of ecosystem-scale carbon dioxide, water vapor, and energy
920 flux densities, *Bull. Am. Meteorol. Soc.*, 82(11), 2415–2434 [online] Available from: <Go to
921 ISI>://000171929700004, 2001a.
- 922 Baldocchi, D., Falge, E. and Wilson, K.: A spectral analysis of biosphere-atmosphere trace gas
923 flux densities and meteorological variables across hour to multi-year time scales, *Agric. For.*
924 *Meteorol.*, 107(1), 1–27, doi:10.1016/s0168-1923(00)00228-8, 2001b.
- 925 Balzarolo, M., Anderson, K., Nichol, C., Rossini, M., Vescovo, L., Arriga, N., Wohlfahrt, G.,
926 Calvet, J.-C., Carrara, A., Cerasoli, S., Cogliati, S., Daumard, F., Eklundh, L., Elbers, J. A.,
927 Evrendilek, F., Handcock, R. N., Kaduk, J., Klumpp, K., Longdoz, B., Matteucci, G., Meroni,
928 M., Montagnani, L., Ourcival, J.-M., Sánchez-Cañete, E. P., Pontailler, J.-Y., Juszczak, R.,
929 Scholes, B. and Martín, M. P.: Ground-Based Optical Measurements at European Flux Sites: A
930 Review of Methods, Instruments and Current Controversies, *Sensors*, 11(12), 7954–7981,
931 doi:10.3390/s110807954, 2011.
- 932 Bauer, M. E.: The role of remote sensing in determining the distribution and yield of crops, *Adv.*
933 *Agron.*, 27, 271–304, doi:10.1016/s0065-2113(08)70012-9, 1975.
- 934 Beget, M. E. and Di Bella, C. M.: Flooding: The effect of water depth on the spectral response of
935 grass canopies, *J. Hydrol.*, 335(3–4), 285–294, doi:10.1016/j.jhydrol.2006.11.018, 2007.
- 936 Bolster, K. L., Martin, M. E. and Aber, J. D.: Determination of carbon fraction and nitrogen
937 concentration in tree foliage by near infrared reflectances: a comparison of statistical methods,
938 *Can. J. For. Res.*, 26(4), 590–600, doi:10.1139/x26-068, 1996.
- 939 Carter, G. A. and Miller, R. L.: Early detection of plant stress by digital imaging within narrow
940 stress-sensitive wavebands, *Remote Sens. Environ.*, 50(3), 295–302, doi:10.1016/0034-
941 4257(94)90079-5, 1994.

942 Chen, S., Hong, X., Harris, C. J. and Sharkey, P. M.: Sparse modeling using orthogonal forest
 943 regression with PRESS statistic and regularization, *IEEE Trans. Syst. Man Cybern.*, 34, 898–
 944 911, 2004.

945 Colwell, J. E.: Vegetation canopy reflectance, *Remote Sens. Environ.*, 3(3), 175–183,
 946 doi:10.1016/0034-4257(74)90003-0, 1974.

947 Dawson, T. P., Curran, P. J., North, P. R. J. and Plummer, S. E.: The Propagation of Foliar
 948 Biochemical Absorption Features in Forest Canopy Reflectance, *Remote Sens. Environ.*, 67(2),
 949 147–159, doi:10.1016/S0034-4257(98)00081-9, 1999.

950 Detto, M., Baldocchi, D. and Katul, G. G.: Scaling Properties of Biologically Active Scalar
 951 Concentration Fluctuations in the Atmospheric Surface Layer over a Managed Peatland,
 952 *Boundary-Layer Meteorol.*, 136(3), 407–430, doi:10.1007/s10546-010-9514-z, 2010.

953 Gamon, J. A., Coburn, C., Flanagan, L. B., Huemmrich, K. F., Kiddle, C., Sanchez-Azofeifa, G.
 954 A., Thayer, D. R., Vescovo, L., Gianelle, D., Sims, D. A., Rahman, A. F. and Pastorello, G. Z.:
 955 SpecNet revisited: bridging flux and remote sensing communities, *Can. J. Remote Sens.*, 36(S2),
 956 S376–S390, doi:10.5589/m10-067, 2010.

957 Gamon, J. A., Serrano, L. and Surfus, J. S.: The Photochemical Reflectance Index: An Optical
 958 Indicator of Photosynthetic Radiation Use Efficiency across Species, Functional Types, and
 959 Nutrient Levels, *Oecologia*, 112(4), 492–501, doi:10.2307/4221805, 1997.

960 Gitelson, A. A. and Merzlyak, M. N.: Remote estimation of chlorophyll content in higher plant
 961 leaves, *Int. J. Remote Sens.*, 18(12), 2691–2697, doi:10.1080/014311697217558, 1997.

962 Hansen, P. M. and Schjoerring, J. K.: Reflectance measurement of canopy biomass and nitrogen
 963 status in wheat crops using normalized difference vegetation indices and partial least squares
 964 regression, *Remote Sens. Environ.*, 86(4), 542–553, doi:http://dx.doi.org/10.1016/S0034-
 965 4257(03)00131-7, 2003.

966 Hatala, J. A., Detto, M., Sonnentag, O., Deverel, S. J., Verfaillie, J. and Baldocchi, D.:
 967 Greenhouse gas (CO₂, CH₄, H₂O) fluxes from drained and flooded agricultural peatlands in the
 968 Sacramento-San Joaquin Delta, *Agric. Ecosyst. Environ.*, 150, 1–18, 2012.

969 Hestir, E. L., Khanna, S., Andrew, M. E., Santos, M. J., Viers, J. H., Greenberg, J. A., Rajapakse,
 970 S. S. and Ustin, S. L.: Identification of invasive vegetation using hyperspectral remote sensing in
 971 the California Delta ecosystem, *Remote Sens. Environ.*, 112(11), 4034–4047,
 972 doi:10.1016/j.rse.2008.01.022, 2008.

973 Hilker, T., Coops, N. C., Nesic, Z., Wulder, M. A. and Black, A. T.: Instrumentation and
 974 approach for unattended year round tower based measurements of spectral reflectance, *Comput.*
 975 *Electron. Agric.*, 56(1), 72–84, doi:10.1016/j.compag.2007.01.003, 2007.

976 Hilker, T., Hall, F. G., Coops, N. C., Black, A. T., Jassal, R., Mathys, A. and Grant, N.:
977 Potentials and limitations for estimating daytime ecosystem respiration by combining tower-
978 based remote sensing and carbon flux measurements, *Remote Sens. Environ.*, 150, 44–52,
979 doi:10.1016/j.rse.2014.04.018, 2014.

980 Inoue, Y., Peñuelas, J., Miyata, A. and Mano, M.: Normalized difference spectral indices for
981 estimating photosynthetic efficiency and capacity at a canopy scale derived from hyperspectral
982 and CO₂ flux measurements in rice, *Remote Sens. Environ.*, 112(1), 156–172,
983 doi:10.1016/j.rse.2007.04.011, 2008.

984 Justice, C. O., Townshend, J. R. G., Holben, B. N. and Tucker, C. J.: Analysis of the phenology
985 of global vegetation using meteorological satellite data, *Int. J. Remote Sens.*, 6(8), 1271–1318,
986 doi:10.1080/01431168508948281, 1985.

987 Kawamura, K., Watanabe, N., Sakanoue, S. and Inoue, Y.: Estimating forage biomass and
988 quality in a mixed sown pasture based on partial least squares regression with waveband
989 selection, *Grassl. Sci.*, 54(3), 131–145, doi:10.1111/j.1744-697X.2008.00116.x, 2008.

990 Knox, S. H., Sturtevant, C., Matthes, J. H., Koteen, L., Verfaillie, J. and Baldocchi, D.:
991 Agricultural peatland restoration: effects of land-use change on greenhouse gas (CO₂ and CH₄)
992 fluxes in the Sacramento-San Joaquin Delta, *Glob. Chang. Biol.*, online ear,
993 doi:10.1111/gcb.12745, 2014.

994 Knyazikhin, Y., Schull, M. A., Stenberg, P., Möttus, M., Rautiainen, M., Yang, Y., Marshak, A.,
995 Latorre Carmona, P., Kaufmann, R. K., Lewis, P., Disney, M. I., Vanderbilt, V., Davis, A. B.,
996 Baret, F., Jacquemoud, S., Lyapustin, A. and Myneni, R. B.: Hyperspectral remote sensing of
997 foliar nitrogen content, *Proc. Natl. Acad. Sci.*, 110(3), E185–E192,
998 doi:10.1073/pnas.1210196109, 2013.

999 Leuning, R., Hughes, D., Daniel, P., Coops, N. and Newnham, G.: A multi-angle spectrometer
1000 for automatic measurement of plant canopy reflectance spectra, *Remote Sens. Environ.*, 103(3),
1001 236–245, doi:10.1016/j.rse.2005.06.016, 2006.

1002 Liu, H. Q. and Huete, A.: A feedback based modification of the NDVI to minimize canopy
1003 background and atmospheric noise, *Ieee Trans. Geosci. Remote Sens.*, 33(3), 814 [online]
1004 Available from: <Go to ISI>://WOS:A1995RB11400033, 1995.

1005 Lloyd, J. and Taylor, J. A.: On the temperature-dependence of soil respiration, *Funct. Ecol.*, 8(3),
1006 315–323, doi:10.2307/2389824, 1994.

1007 Main, R., Cho, M. A., Mathieu, R., O’Kennedy, M. M., Ramoelo, A. and Koch, S.: An
1008 investigation into robust spectral indices for leaf chlorophyll estimation, *Isprs J. Photogramm.*
1009 *Remote Sens.*, 66(6), 751–761, doi:10.1016/j.isprs.2011.08.001, 2011.

1010 Mevik, B.-H., Wehrens, R. and Liland, K. H.: pls, [online] Available from: [http://cran.r-](http://cran.r-project.org/web/packages/pls/pls.pdf)
1011 [project.org/web/packages/pls/pls.pdf](http://cran.r-project.org/web/packages/pls/pls.pdf), 2013.

1012 Moffat, A. M., Papale, D., Reichstein, M., Hollinger, D. Y., Richardson, A. D., Barr, A. G.,
1013 Beckstein, C., Braswell, B. H., Churkina, G., Desai, A. R., Falge, E., Gove, J. H., Heimann, M.,
1014 Hui, D. F., Jarvis, A. J., Kattge, J., Noormets, A. and Stauch, V. J.: Comprehensive comparison
1015 of gap-filling techniques for eddy covariance net carbon fluxes, *Agric. For. Meteorol.*, 147(3-4),
1016 209–232, doi:10.1016/j.agrformet.2007.08.011, 2007.

1017 Moncrieff, J. B., Malhi, Y. and Leuning, R.: Biosphere-atmosphere exchange of CO₂ in relation
1018 to climate: a cross-biome analysis across multiple time scales, *Glob. Chang. Biol.*, 2(3), 231–
1019 240, doi:10.1111/j.1365-2486.1996.tb00075.x, 1996.

1020 Nicodemus, F. E., Richmond, J. C., Hsia, J. J., Ginsberg, I. W. and Limeris, T.: Geometrical
1021 Considerations and Nomenclature for Reflectance, Washington, DC., 1977.

1022 Ollinger, S. V., Smith, M. L., Martin, M. E., Hallett, R. A., Goodale, C. L. and Aber, J. D.:
1023 Regional variation in foliar chemistry and N cycling among forests of diverse history and
1024 composition, *Ecology*, 83(2), 339–355, doi:10.1890/0012-
1025 9658(2002)083[0339:RVIFCA]2.0.CO;2, 2002.

1026 Papale, D., Reichstein, M., Aubinet, M., Canfora, E., Bernhofer, C., Kutsch, W., Longdoz, B.,
1027 Rambal, S., Valentini, R., Vesala, T. and Yakir, D.: Towards a standardized processing of Net
1028 Ecosystem Exchange measured with eddy covariance technique: algorithms and uncertainty
1029 estimation, *Biogeosciences*, 3(4), 571–583 [online] Available from: <Go to
1030 ISI>://WOS:000243785300013, 2006.

1031 Potter, C. S., Randerson, J. T., Field, C. B., Matson, P. A., Vitousek, P. M., Mooney, H. A. and
1032 Klooster, S. A.: Terrestrial ecosystem production: A process model based on global satellite and
1033 surface data, *Global Biogeochem. Cycles*, 7(4), 811–841, doi:10.1029/93GB02725, 1993.

1034 Reichstein, M., Falge, E., Baldocchi, D., Papale, D., Aubinet, M., Berbigier, P., Bernhofer, C.,
1035 Buchmann, N., Gilmanov, T., Granier, A., Grunwald, T., Havrankova, K., Ilvesniemi, H.,
1036 Janous, D., Knohl, A., Laurila, T., Lohila, A., Loustau, D., Matteucci, G., Meyers, T., Miglietta,
1037 F., Ourcival, J. M., Pumpanen, J., Rambal, S., Rotenberg, E., Sanz, M., Tenhunen, J., Seufert, G.,
1038 Vaccari, F., Vesala, T., Yakir, D. and Valentini, R.: On the separation of net ecosystem exchange
1039 into assimilation and ecosystem respiration: review and improved algorithm, *Glob. Chang. Biol.*,
1040 11(9), 1424–1439, doi:10.1111/j.1365-2486.2005.001002.x, 2005.

1041 Reichstein, M., Papale, D., Valentini, R., Aubinet, M., Bernhofer, C., Knohl, A., Laurila, T.,
1042 Lindroth, A., Moors, E., Pilegaard, K. and Seufert, G.: Determinants of terrestrial ecosystem
1043 carbon balance inferred from European eddy covariance flux sites, *Geophys. Res. Lett.*, 34(1),
1044 n/a–n/a, doi:10.1029/2006GL027880, 2007.

1045 Rossini, M., Meroni, M., Migliavacca, M., Manca, G., Cogliati, S., Busetto, L., Picchi, V.,
1046 Cescatti, A., Seufert, G. and Colombo, R.: High resolution field spectroscopy measurements for
1047 estimating gross ecosystem production in a rice field, *Agric. For. Meteorol.*, 150(9), 1283–1296,
1048 doi:10.1016/j.agrformet.2010.05.011, 2010.

- 1049 Rouse, J. W., Haas, R. H., Schell, J. A. and Deering, D. W.: Monitoring vegetation systems in
1050 the Great Plains with ERTS, in 3rd ERTS Symposium, pp. 309–317, NASA SP-351 I., 1973.
- 1051 Running, S. W., Baldocchi, D. D., Turner, D. P., Gower, S. T., Bakwin, P. S. and Hibbard, K. A.:
1052 A global terrestrial monitoring network integrating tower fluxes, flask sampling, ecosystem
1053 modeling and EOS satellite data, *Remote Sens. Environ.*, 70(1), 108–127, doi:10.1016/s0034-
1054 4257(99)00061-9, 1999.
- 1055 Running, S. W. and Nemani, R. R.: Relating seasonal patterns of the AVHRR vegetation index
1056 to simulated photosynthesis and transpiration of forests in different climates, *Remote Sens.*
1057 *Environ.*, 24(2), 347–367, 1988.
- 1058 Ryu, Y., Baldocchi, D. D., Verfaillie, J., Ma, S., Falk, M., Ruiz-Mercado, I., Hehn, T. and
1059 Sonnentag, O.: Testing the performance of a novel spectral reflectance sensor, built with light
1060 emitting diodes (LEDs), to monitor ecosystem metabolism, structure and function, *Agric. For.*
1061 *Meteorol.*, 150(12), 1597–1606, doi:http://dx.doi.org/10.1016/j.agrformet.2010.08.009, 2010a.
- 1062 Ryu, Y., Nilson, T., Kobayashi, H., Sonnentag, O., Law, B. E. and Baldocchi, D. D.: On the
1063 correct estimation of effective leaf area index: Does it reveal information on clumping effects?,
1064 *Agric. For. Meteorol.*, 150(3), 463–472, doi:10.1016/j.agrformet.2010.01.009, 2010b.
- 1065 Schaepman-Strub, G., Schaepman, M. E., Painter, T. H., Dangel, S. and Martonchik, J. V.:
1066 Reflectance quantities in optical remote sensing—definitions and case studies, *Remote Sens.*
1067 *Environ.*, 103(1), 27–42, doi:10.1016/j.rse.2006.03.002, 2006.
- 1068 Schmidtlein, S., Zimmermann, P., Schüpferling, R. and Weiß, C.: Mapping the floristic
1069 continuum: Ordination space position estimated from imaging spectroscopy, *J. Veg. Sci.*, 18(1),
1070 131–140, doi:10.1111/j.1654-1103.2007.tb02523.x, 2007.
- 1071 Schotanus, P., Nieuwstadt, F. T. M. and Debruin, H. A. R.: Temperature measurement with a
1072 sonic anemometer and its application to heat and moisture fluxes, *Boundary-Layer Meteorol.*,
1073 26(1), 81–93 [online] Available from: <Go to ISI>://WOS:A1983QX37400006, 1983.
- 1074 Serbin, S. P., Dillaway, D. N., Kruger, E. L. and Townsend, P. A.: Leaf optical properties reflect
1075 variation in photosynthetic metabolism and its sensitivity to temperature, *J. Exp. Bot.*, 63(1),
1076 489–502, doi:10.1093/jxb/err294, 2012.
- 1077 Serbin, S. P., Singh, A., McNeil, B. E., Kingdon, C. C. and Townsend, P. A.: Spectroscopic
1078 determination of leaf morphological and biochemical traits for northern temperate and boreal tree
1079 species, *Ecol. Appl.*, doi:10.1890/13-2110.1, 2014.
- 1080 Sims, D. A., Rahman, A. F., Cordova, V. D., Baldocchi, D. D., Flanagan, L. B., Goldstein, A. H.,
1081 Hollinger, D. Y., Misson, L., Monson, R. K., Schmid, H. P., Wofsy, S. C. and Xu, L.: Midday
1082 values of gross CO₂ flux and light use efficiency during satellite overpasses can be used to
1083 directly estimate eight-day mean flux, *Agric. For. Meteorol.*, 131(1-2), 1–12,
1084 doi:10.1016/j.agrformet.2005.04.006, 2005.

1085 Smith, M.-L., Ollinger, S. V, Martin, M. E., Aber, J. D., Hallett, R. A. and Goodale, C. L.: Direct
 1086 estimation of aboveground forest productivity through hyperspectral remote sensing of canopy
 1087 nitrogen, *Ecol. Appl.*, 12(5), 1286–1302, doi:10.1890/1051-
 1088 0761(2002)012[1286:DEOAFP]2.0.CO;2, 2002.

1089 Sonnentag, O., Detto, M., Runkle, B. R. K., Teh, Y. A., Silver, W. L., Kelly, M. and Baldocchi,
 1090 D. D.: Carbon dioxide exchange of a pepperweed (*Lepidium latifolium*L.) infestation: How do
 1091 flowering and mowing affect canopy photosynthesis and autotrophic respiration?, *J. Geophys.*
 1092 *Res.*, 116(G1), doi:10.1029/2010jg001522, 2011a.

1093 Sonnentag, O., Detto, M., Vargas, R., Ryu, Y., Runkle, B. R. K., Kelly, M. and Baldocchi, D. D.:
 1094 Tracking the structural and functional development of a perennial pepperweed (*Lepidium*
 1095 *latifolium* L.) infestation using a multi-year archive of webcam imagery and eddy covariance
 1096 measurements, *Agric. For. Meteorol.*, 151(7), 916–926, doi:10.1016/j.agrformet.2011.02.011,
 1097 2011b.

1098 Stoy, P. C., Richardson, A. D., Baldocchi, D. D., Katul, G. G., Stanovick, J., Mahecha, M. D.,
 1099 Reichstein, M., Detto, M., Law, B. E., Wohlfahrt, G., Arriga, N., Campos, J., McCaughey, J. H.,
 1100 Montagnani, L., Paw U, K. T., Sevanto, S. and Williams, M.: Biosphere-atmosphere exchange of
 1101 CO₂ in relation to climate: a cross-biome analysis across multiple time scales, *Biogeosciences*,
 1102 6(10), 2297–2312, doi:10.5194/bg-6-2297-2009, 2009.

1103 Tucker, C. J., Townshend, J. R. G. and Goff, T. E.: African land-cover classification using
 1104 satellite data, *Science* (80-), 227(4685), 369–375, 1985.

1105 Ustin, S. L., Roberts, D. A., Gamon, J. A., Asner, G. P. and Green, R. O.: Using Imaging
 1106 Spectroscopy to Study Ecosystem Processes and Properties, *Bioscience*, 54(6), 523–534,
 1107 doi:10.1641/0006-3568(2004)054[0523:UISTSE]2.0.CO;2, 2004.

1108 Verhoef, W. and Bach, H.: Coupled soil–leaf–canopy and atmosphere radiative transfer modeling
 1109 to simulate hyperspectral multi-angular surface reflectance and TOA radiance data, *Remote*
 1110 *Sens. Environ.*, 109(2), 166–182, doi:10.1016/j.rse.2006.12.013, 2007.

1111 Webb, E. K., Pearman, G. I. and Leuning, R.: Correction of flux measurements for density
 1112 effects due to heat and water-vapor transfer, *Q. J. R. Meteorol. Soc.*, 106(447), 85–100 [online]
 1113 Available from: <Go to ISI>://WOS:A1980JD79200007, 1980.

1114 Wold, S., Sjostrom, M. and Eriksson, L.: PLS-regression: a basic tool of chemometrics,
 1115 *Chemom. Intell. Lab. Syst.*, 58, 109–130, 2001.

1116 Yang, X., Tang, J. and Mustard, J. F.: Beyond leaf color: Comparing camera-based phenological
 1117 metrics with leaf biochemical, biophysical, and spectral properties throughout the growing
 1118 season of a temperate deciduous forest, *J. Geophys. Res. Biogeosciences*, 119(3), 181–191,
 1119 doi:10.1002/2013JG002460, 2014.

1120 Ye, X., Sakai, K., Sasao, A. and Asada, S.: Estimation of citrus yield from canopy spectral
1121 features determined by airborne hyperspectral imagery, *Int. J. Remote Sens.*, 30(18), 4621–4642,
1122 doi:10.1080/01431160802632231, 2009.

1123

1124

1125 **Table 1. Fit statistics for the bootstrapped PLSR model.** The mean R^2 and root mean squared
 1126 error (RMSE) is provided for the PLSR Calibration fitting (Cal) and the calibration Evaluation
 1127 (Eval) during the PLSR model development, conducted with 80% of the total dataset. [Units for](#)
 1128 [instantaneous fluxes are \$\mu\text{mol m}^{-2} \text{s}^{-1}\$, and for daily, weekly, and monthly values are \$\text{g-C m}^{-2}\$.](#) In
 1129 general, models with daily-integrated GPP and NEE had the best fit compared with models that
 1130 fit the flux data from other timescales. The PLSR fit for GPP using the hyperspectral reflectance
 1131 data tended to outperform the fit of NEE across the datasets and models. The statistical fit of the
 1132 PLSR models was [higher at the Rice site compared with the Pasture.](#)

		R^2 Cal	R^2 Eval	RMSE Cal	RMSE Eval	Components
Both sites	GPP inst	0.87	0.64	3.34	4.74	7
	GPP daily	0.87	0.69	1.42	1.96	6
	GPP wkly	0.86	0.69	10.35	13.82	6
	GPP mthly	0.63	0.24	45.47	44.75	6
	NEE inst	0.84	0.64	3.30	4.39	6
	NEE daily	0.84	0.66	1.43	1.87	6
	NEE wkly	0.83	0.65	10.34	13.21	6
	NEE mthly	0.81	0.64	42.11	51.88	6
Pasture	GPP inst	0.94	0.49	1.36	3.49	7
	GPP daily	0.97	0.56	0.43	1.53	8
	GPP wkly	0.53	0.38	11.64	10.15	3
	GPP mthly	0.91	0.42	22.96	52.43	7
	NEE inst	0.43	0.33	3.56	2.52	2
	NEE daily	0.38	0.30	1.40	0.91	2
	NEE wkly	0.44	0.29	8.47	6.42	3
	NEE mthly	0.79	0.36	22.81	30.49	6
Rice	GPP inst	0.85	0.61	4.34	5.92	5
	GPP daily	0.92	0.65	1.34	2.58	6
	GPP wkly	0.84	0.67	13.32	17.06	4
	GPP mthly	0.89	0.68	10.96	16.95	5
	NEE inst	0.77	0.58	4.88	5.66	4
	NEE daily	0.86	0.60	1.68	2.52	5
	NEE wkly	0.85	0.59	11.82	17.88	5

Jaclyn Matthes 7/16/2015 11:08 AM

Deleted: significantly

	NEE mthly	0.80	0.64	56.50	67.93	4
--	-----------	------	------	-------	-------	---

1135 **Table 2. Independent validation dataset fit for mean PLSR models.** We calculated the R^2 and
 1136 bias between the predicted CO₂ flux variables with the mean PLSR models and the actual
 1137 measurements from the 20% of data left for Independent Validation. [Units for instantaneous](#)
 1138 [fluxes are \$\mu\text{mol m}^{-2} \text{s}^{-1}\$, and for daily, weekly, and monthly values are \$\text{g-C m}^{-2}\$.](#) The highest
 1139 predictive fit for the PLSR models was achieved with the dataset that included the Rice data
 1140 only.

		R^2		Bias	
		NEE	GPP	NEE	GPP
Both sites	Inst	0.51	0.42	-1.63	3.89
	Daily	0.52	0.52	-0.41	1.60
	Weekly	0.55	0.62	-3.31	9.75
	Monthly	0.57	0.27	-11.92	31.51
Pasture	Inst	0.53	0.24	-2.28	5.10
	Daily	0.44	0.45	-0.56	2.79
	Weekly	0.51	0.54	-1.96	15.94
	Monthly	0.43	0.47	-14.18	76.86
Rice	Inst	0.51	0.40	-1.41	2.73
	Daily	0.65	0.50	-0.89	0.58
	Weekly	0.69	0.62	-2.35	0.21
	Monthly	0.41	0.45	-18.56	4.60

1141

1142

Table 3. Comparison of SVIs and PLSR model skill. We evaluated the ability of the commonly used standardized vegetation indices (SVIs) to predict GPP and NEE in comparison with the PLSR models. Here we show results for the widely used MODIS NDVI (NDVI_{MOD}) and the red-edge NDVI (NDVI_{re}), which was the SVI that achieved the highest skill at predicting GPP and NEE. Results from all SVIs tested in this study are included as Supplementary Table 1.

Site	Flux	NDVI _{MOD} fit	NDVI _{re} fit	PLSR fit	NDVI _{MOD} pred	NDVI _{re} pred	PLSR pred
All	GPP_inst	0.50	0.57	0.87	0.18	0.22	0.42
All	GPP_day	0.55	0.65	0.87	0.44	0.53	0.52
All	GPP_week	0.56	0.64	0.86	0.42	0.50	0.62
All	GPP_month	0.49	0.56	0.63	0.32	0.38	0.27
All	NEE_inst	0.49	0.57	0.84	0.50	0.57	0.51
All	NEE_day	0.45	0.54	0.84	0.51	0.58	0.52
All	NEE_week	0.48	0.56	0.83	0.53	0.59	0.55
All	NEE_month	0.53	0.58	0.81	0.54	0.59	0.57
Pasture	GPP_inst	0.29	0.38	0.94	0.09	0.13	0.24
Pasture	GPP_day	0.35	0.45	0.97	0.26	0.34	0.45
Pasture	GPP_week	0.29	0.38	0.53	0.22	0.30	0.54
Pasture	GPP_month	0.18	0.25	0.91	0.13	0.19	0.47
Pasture	NEE_inst	0.31	0.40	0.43	0.30	0.39	0.53
Pasture	NEE_day	0.31	0.41	0.38	0.26	0.35	0.44
Pasture	NEE_week	0.29	0.36	0.44	0.25	0.31	0.51
Pasture	NEE_month	0.20	0.25	0.79	0.17	0.22	0.43
Rice	GPP_inst	0.46	0.54	0.85	0.48	0.49	0.4
Rice	GPP_day	0.56	0.69	0.92	0.57	0.62	0.5
Rice	GPP_week	0.60	0.72	0.84	0.62	0.65	0.62
Rice	GPP_month	0.59	0.68	0.89	0.60	0.63	0.45
Rice	NEE_inst	0.47	0.56	0.77	0.49	0.52	0.51
Rice	NEE_day	0.49	0.60	0.86	0.51	0.55	0.65
Rice	NEE_week	0.54	0.64	0.85	0.56	0.58	0.69
Rice	NEE_month	0.60	0.69	0.8	0.63	0.64	0.41

1149 **Figure captions**

1150 **Figure 1. Canopy hyperspectral field collection dates.** This analysis synthesized canopy
1151 hyperspectral reflectance measurements collected from 2010-2014 at Pasture and Rice sites in
1152 the Sacramento-San Joaquin Delta in Northern California. On each sampling date we collected
1153 nine individual canopy hyperspectral reflectance replicates at the Pasture site and five individual
1154 reflectance replicates at the Rice site.

1155

1156 **Figure 2. Instantaneous gross primary productivity (GPP) and daily net CO₂ flux on the**
1157 **hyperspectral canopy reflectance sampling dates.** Both the Pasture and the Rice exhibited
1158 strong seasonal patterns with peak CO₂ uptake mid-year. However, the Pasture experienced peak
1159 CO₂ uptake that preceded the peak for the Rice, where the maximum CO₂ uptake occurred in
1160 March-April for the Pasture and in July-August for the Rice.

1161

1162 **Figure 3. Daily variability in measured canopy hyperspectral reflectance during**
1163 **phenological events. a-b)** Daily measured hyperspectral canopy reflectance for the Pasture and
1164 Rice sites when the canopy was closed and green, at the Pasture on 10 April 2014 and the Rice
1165 on 31 July 2013. Reflectance was very low in the visible wavelengths due to canopy absorption,
1166 but quite large in the near infrared reflectance with a high amount of variability. Both sites had
1167 spectral peaks that corresponded to green reflectance (~550 nm) and troughs that corresponded to
1168 spectral absorption in red reflectance (~675 nm). **c)** During the white flowering of the
1169 pepperweed plants, the measured reflectance changed significantly, due to the higher albedo of
1170 the bright white flowers. There was much higher reflectance across the spectrum during this
1171 time, and the white flowers obfuscated reflectance in the wavelengths that corresponded to plant

1172 productivity. **d)** There was a similar but not as dramatic shift in increased albedo particularly
1173 across the visible wavelengths from green to red reflectance during the rice seeding and
1174 senescence as the canopy dried before harvest. However an important distinction between this
1175 phenological event and the white flowering at the Pasture is that the productivity of the rice
1176 plants was quite low at this time, in contrast with the higher productivity of the pepperweed
1177 during flowering.

1178

1179 **Figure 4. Inter-annual and daily variability at narrow-band green, red, and near-infrared**
1180 **(NIR) reflectance. a-b)** Inter-annual variability in measured canopy green reflectance at 550 ± 5
1181 nm, where the points are the site mean and the bars represent one standard deviation for each
1182 sampling date. The green reflectance at the Pasture was relatively uniform throughout the year,
1183 due to the presence of either grass or pepperweed canopy for most of the year. There was more
1184 intra-site variability in reflectance during the summer when the pepperweed canopy was active,
1185 since at some locations the white flowers of the pepperweed plant can complicate the green
1186 reflectance spectrum. The green reflectance at the Rice had more inter-annual variability but a
1187 more discernible seasonal pattern within each year, where the trough in green reflectance tended
1188 to occur mid-summer. **c-d)** These plots show red reflectance at 662 ± 5 nm at each site, which
1189 corresponds to the absorption wavelength of chlorophyll b. Both sites demonstrated a seasonal
1190 pattern, where the minimum in red reflectance occurred in late spring at the Pasture and in late
1191 summer at the Rice, corresponding to the times of peak plant growth at each site. Again, the
1192 Pasture had more intra-site variability, particularly during the summer months when pepperweed
1193 is active. **e-f)** Here we plot the near infrared (NIR) reflectance at 800 ± 5 nm for the two sites. NIR
1194 reflectance at the Pasture had no strong seasonal pattern, with a constant mean throughout the

1195 year and across years. The rice demonstrated a stronger pattern across the season, with less NIR
1196 reflectance early in the growing season when the canopy was developing, with higher NIR
1197 reflectance as the crop achieved a full canopy later in the summer. At both sites, intra-site
1198 variability in NIR reflectance was much higher than the variability in the reflectance in the
1199 visible spectrum.

1200

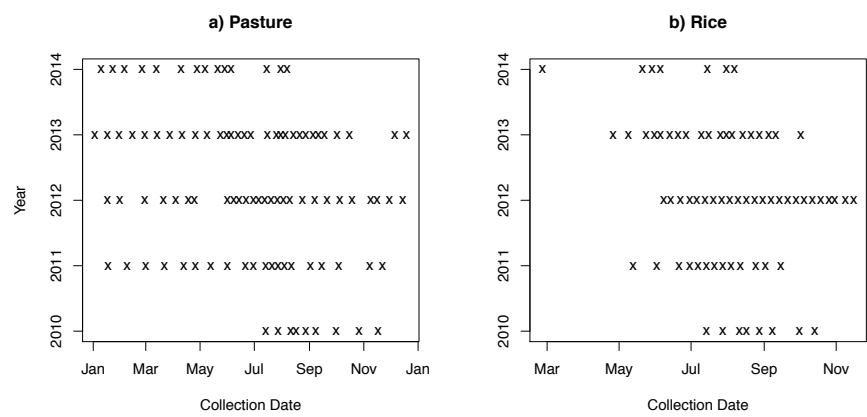
1201 **Figure 5. Variable importance of projection (VIP) statistics for bootstrapped partial least-**
1202 **squared regression (PLSR) modeling coefficients.** Here we show the variable importance of
1203 projection (VIP) statistics for the mean bootstrapped PLSR models, fitted to the GPP and NEE
1204 flux datasets. The VIP statistic describes the relative contribution of each wavelength to the
1205 predictive power of the PLSR model across all final PLSR model components. Across all
1206 models, the visible wavelengths (400-700nm) were most important for prediction at shorter
1207 timescales of integrated flux, while the infrared wavelengths (700-900nm) became increasingly
1208 important at longer integrated flux intervals. This pattern is particularly apparent within the
1209 PLSR model for GPP fitted across All the data (Figure 5a), where there was a dramatic shift in
1210 the VIP statistics between the weekly- and monthly-integrated flux prediction and the infrared
1211 wavelengths become much more important for prediction at longer timescales. This pattern was
1212 also apparent with the PLSR models developed using the Pasture data only. The PLSR models
1213 developed for the Rice data only (Figures 5e-f) had the least variation for fluxes integrated at
1214 different timescales.

1215

1216 **Figure 6. Predictive ability of PLSR models on independent validation dataset.** The mean
1217 PLSR models determined through the bootstrapping routine were tested on the Independent

Validation dataset, which was composed of 20% of the original data that was separated from the model calibration process. Here the independent validation is presented for instantaneous and daily NEE and GPP flux for the exercises with all the data, Pasture only, and Rice only. The regression line between the predicted and actual variables is black, the 1:1 line is dashed, the 95% credible interval of the regression are the curved dotted lines, and the 95% prediction interval are the grey lines.

Figure 7. Predictive power of measured hyperspectral reflectance at increasing CO₂ flux integration intervals. We examined the ability of PLSR modeling with the hyperspectral reflectance data to predict instantaneous and daily-, weekly-, and monthly-integrated NEE and GPP at **a)** both sites with the entire dataset, **b)** the Pasture only, and **c)** the Rice only. For all three cases, the measured hyperspectral reflectance had the highest correlation with weekly-integrated GPP flux. The time interval with the highest predictive power for NEE flux was less variable across different timescales within each modeling exercise, and there was not a strong improvement to using one particular timescale to model NEE with the hyperspectral reflectance data.

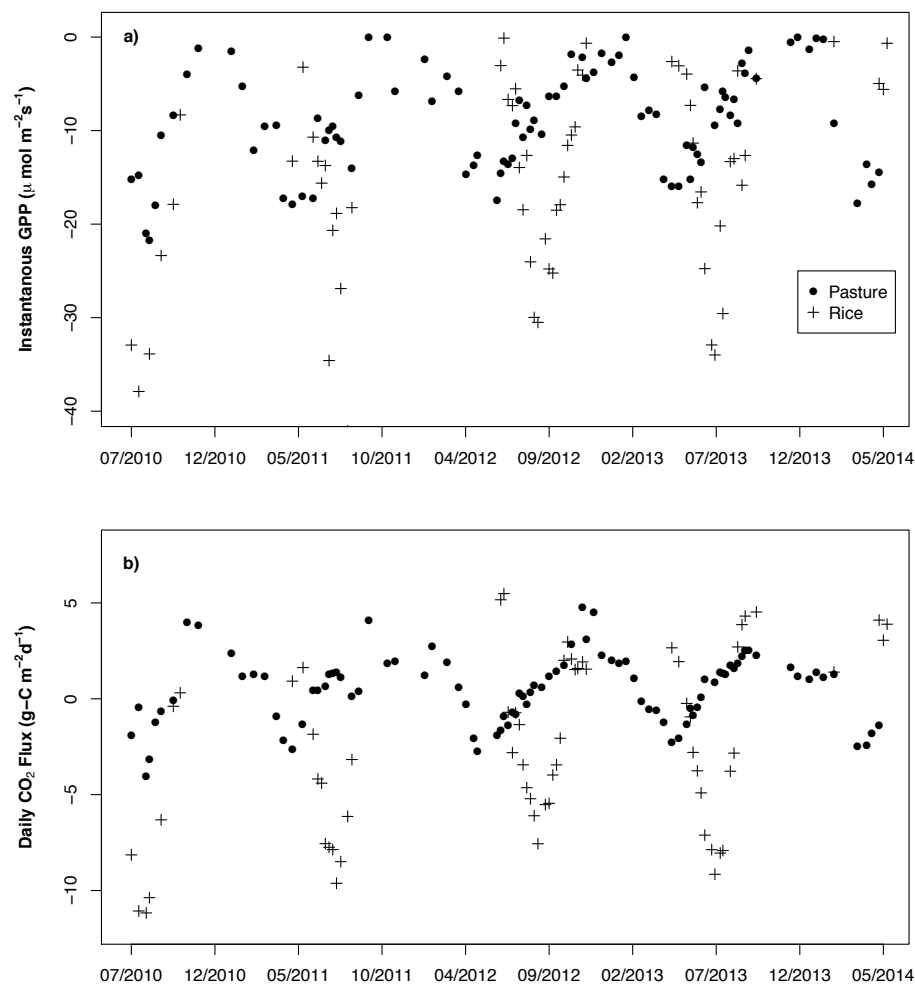


1237

1238

FIGURE 2

Jaclyn Matthes 7/16/2015 11:08 AM
Formatted: Not Highlight



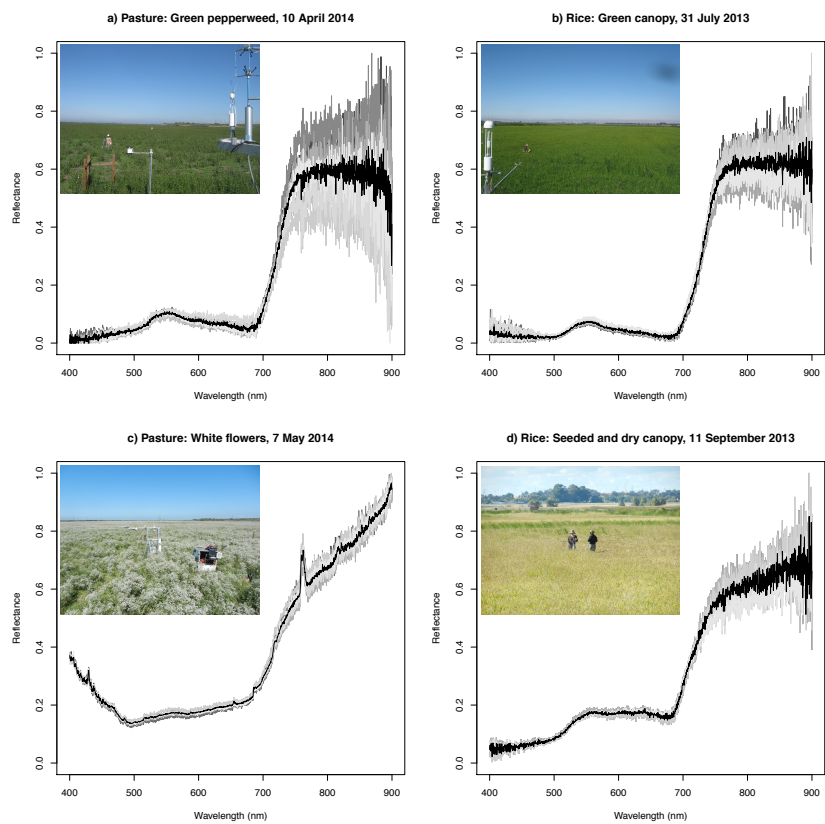
1240

1241

1242

1243

1244



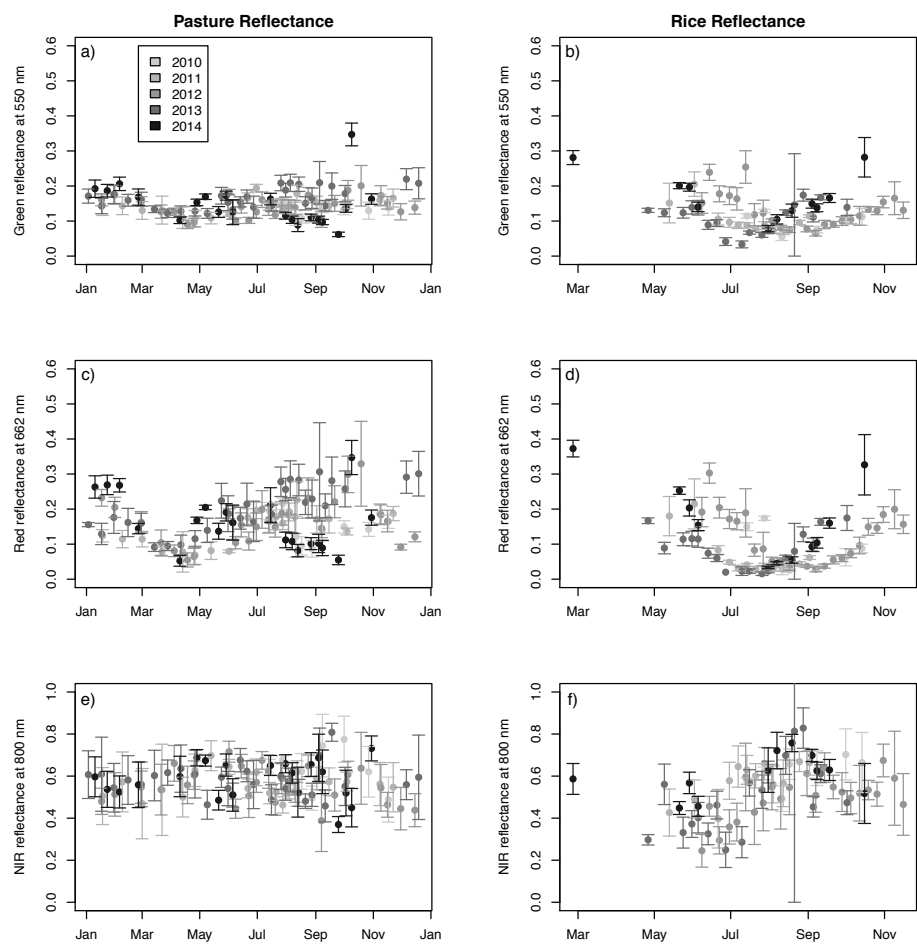
1246

1247

1248

1249

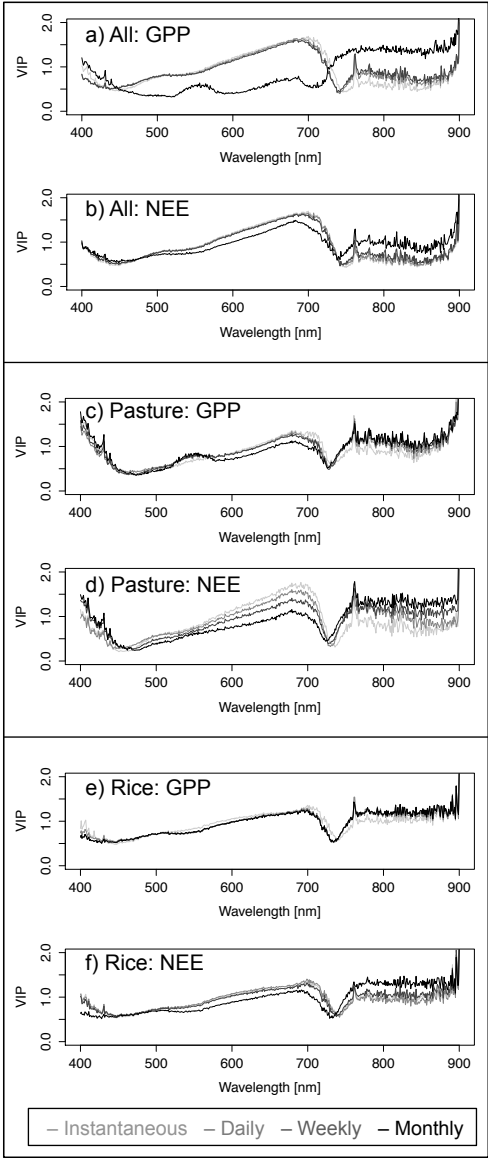
1250



1252

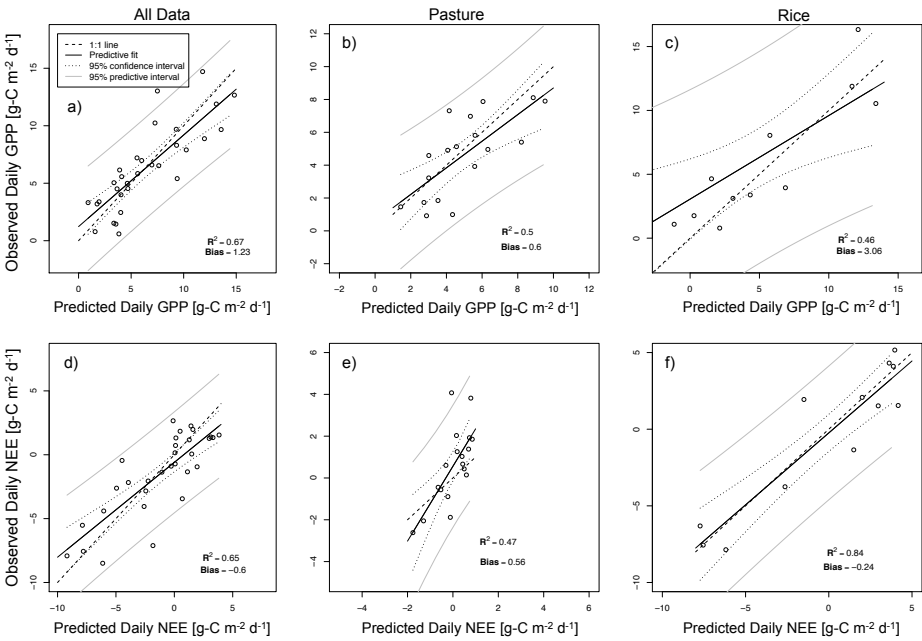
1253

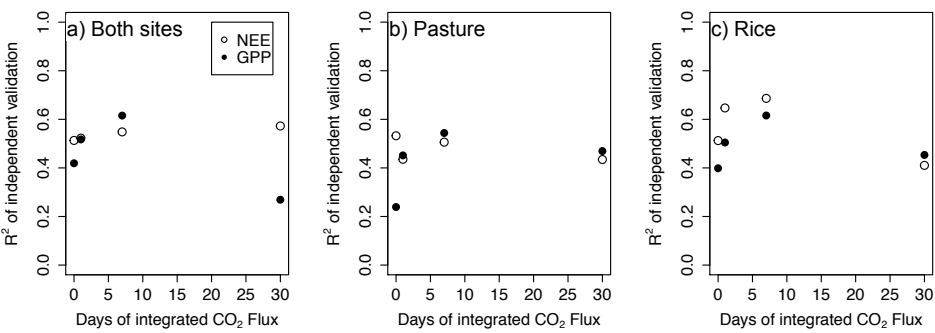
1254



1256

1257





1261

1262